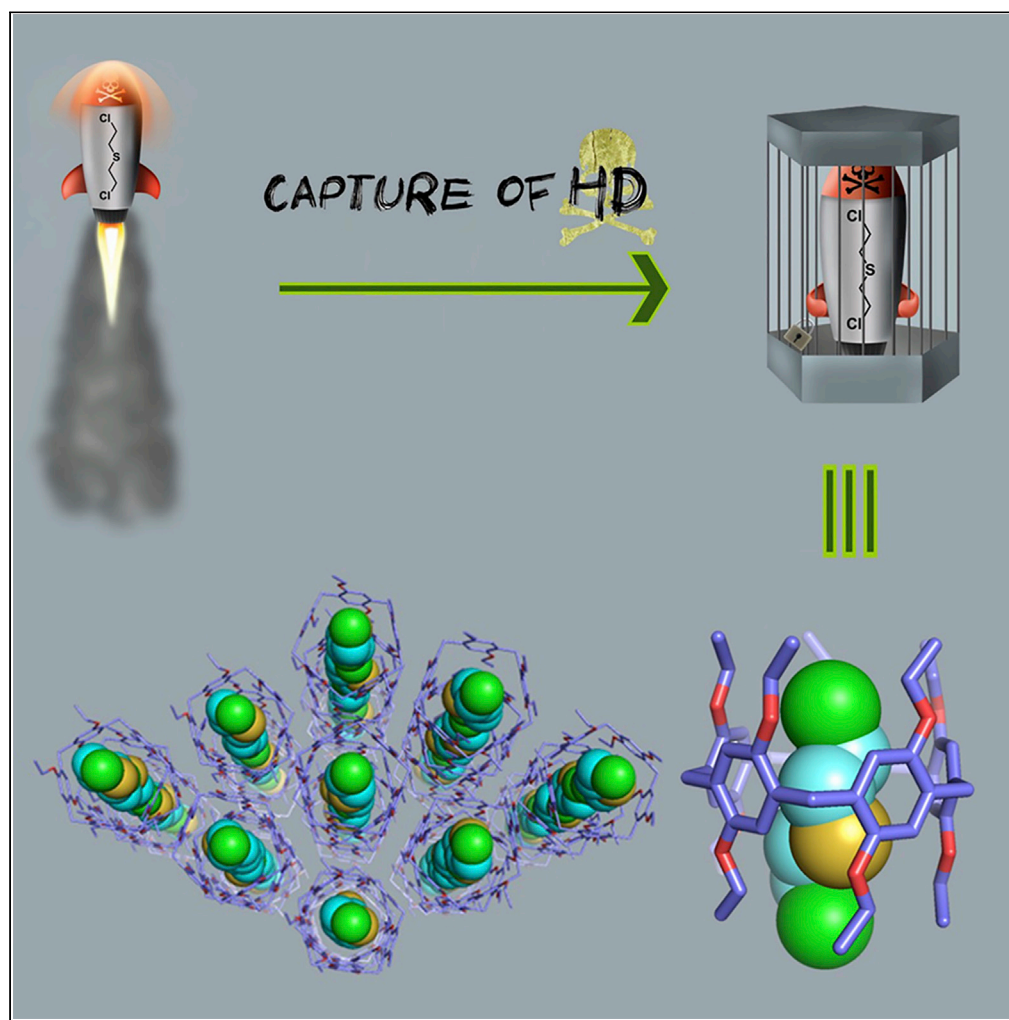**Article**

Capture of Sulfur Mustard by Pillar[5]arene: From Host-Guest Complexation to Efficient Adsorption Using Nonporous Adaptive Crystals

Bin Li, Shuo Li, Bin Wang, Zhao Meng, Yongan Wang, Qingbin Meng, Chunju Li

nankaimqb@sina.com (Q.M.)
cjli@shu.edu.cn (C.L.)

HIGHLIGHTS

Strong binding of sulfur mustard (SM) and its simulants by pillar[5] arenes (EtP5)

Effective capture of SM simulants vapor by activated crystalline materials of EtP5

The adsorption of SM simulants vapor induces a crystal structure transformation

The contained SM simulants can be stabilized in the crystals for at least half a year

Article

Capture of Sulfur Mustard by Pillar[5]arene: From Host-Guest Complexation to Efficient Adsorption Using Nonporous Adaptive Crystals

Bin Li,[1,2,3] Shuo Li,[1] Bin Wang,[3] Zhao Meng,[2] Yongan Wang,[2] Qingbin Meng,[2,*] and Chunju Li[1,3,4,*]

SUMMARY

Sulfur mustard (SM) has been the most frequently used chemical warfare agent. Here, we present the efficient containment of SM and its simulants by *per*-ethylated pillar[5]arene (EtP5). EtP5 exhibited strong binding abilities toward SM and its simulants not only in solution but also in the solid state. The association constant (K_a) between SM and EtP5 was determined as $(6.2 \pm 0.6) \times 10^3 \, M^{-1}$ in *o*-xylene-d_{10}. Single crystal structure of SM@EtP5 showed that a 1:1 inclusion complex was formed, which was driven by multiple C–H$\cdots\pi$/Cl/S and S$\cdots\pi$ interactions. In addition, activated crystal materials of EtP5 (EtP5α) could effectively adsorb SM simulants at solid-vapor phase; powder X-ray diffraction patterns and host-guest crystal structures indicated that the uptake process triggered a solid-state structural transformation. More interestingly, the captured guest molecules could be stably contained in EtP5α for at least 6 months in air at room temperature.

INTRODUCTION

Sulfur mustard (bis(2-chloroethyl)sulfide, SM) is a well-known chemical warfare agent that was first used in World War I (Evison et al., 2001; Szinicz, 2005; Wattana and Bey, 2009). It is referred to several other names (e.g., H, HD, lost, Yperite, and yellow cross liquid) and is the most frequently used chemical warfare agent based on its ease of preparation and its ability to be stored in large quantities. To date, the number of casualties due to SM is greater than the total number of casualties from all other chemical weapons (Szinicz, 2005). Consequently, SM has been called the "King of war gases." As a powerful blistering agent or vesicant, SM can cause serious damage to eyes, skin, and lungs. Moreover, as an active alkylating agent, it can form a highly reactive three-membered cationic sulfonium intermediate that reacts with DNA bases (Fruton et al., 1946). Despite the development of more toxic chemical weapons (e.g., nerve agents) after SM, the latter is still regarded as one of the most efficient chemical agents in modern warfare (e.g., in warfare of Egypt against Yemen [1960s], Iraq against Iran, Kurds [1980s], and Sudan against insurgents [1990s]) and terrorist threats/attacks.

Therefore, considerable efforts have been devoted to exploring the complexation (Wang et al., 2013), sensing/detection (Jang et al., 2015; Kumar and Anslyn, 2013), and detoxification (Liu et al., 2017; Bobbitt et al., 2017; Decoste and Peterson, 2014) of SM or in most cases its structurally similar molecules. Additionally, capture of other toxic sulfur compounds such as hydrogen sulfide (H_2S) and sulfur dioxide (SO_2) by metal-organic frameworks (MOFs), zeolites, and carbon-based materials has been demonstrated (Shah et al., 2017; Tchalala et al., 2019; Islamoglu et al., 2020). It is significantly important to develop effective absorption materials for protection from SM damage. However, simple and straightforward physical adsorption materials for SM have been rarely reported. As is well known, it is a powerful strategy to utilize host-guest encapsulation to construct adsorption materials due to the preorganized cavities and multivalent binding sites of the molecular *containers* (Alsbaiee et al., 2016; Mei et al., 2019; Yu et al., 2012; Wang et al., 2009; Kim et al., 2014; Chen et al., 2013; Schneider et al., 2016; Ajami and Rebek, 2013). To the best of our knowledge, strong interactions of SM, or its stimulants, by macrocyclic hosts have not been demonstrated, because traditional macrocycles have no efficient recognition sites to interact with the small and neutral SM.

As detailed below, we report surprisingly strong interactions of SM by *per*-ethylated pillar[5]arene (EtP5) and efficient containment of SM and its simulants by activated crystalline materials of EtP5 (EtP5α). Pillar[*n*]arenes have been regarded as an important family of supramolecular macrocycles (Ogoshi et al.,

[1]College of Science, Center for Supramolecular Chemistry and Catalysis, Shanghai University, Shanghai 200444, P. R. China

[2]State Key Laboratory of Toxicology and Medical Countermeasures, Beijing Institute of Pharmacology and Toxicology, Beijing 100850, P. R. China

[3]Key Laboratory of Inorganic-Organic Hybrid Functional Material Chemistry, Ministry of Education, Tianjin Key Laboratory of Structure and Performance for Functional Molecules, College of Chemistry, Tianjin Normal University, Tianjin 300387, P. R. China

[4]Lead Contact

*Correspondence:
nankaimqb@sina.com (Q.M.),
cjli@shu.edu.cn (C.L.)

https://doi.org/10.1016/j.isci.2020.101443
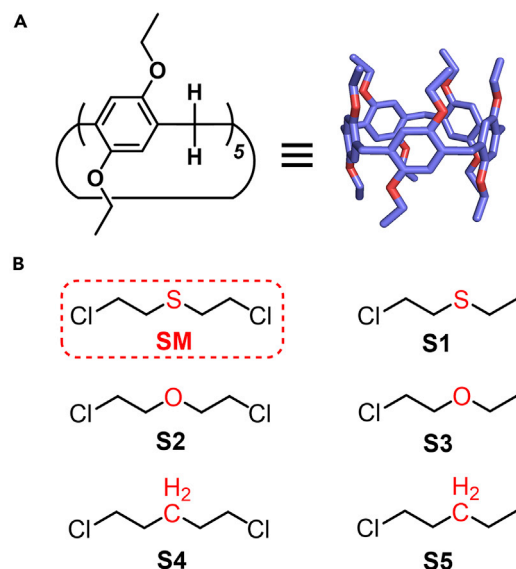
A

B

Figure 1. Schematic Illustration of Compounds Used in This Study

(A) Structures of EtP5 host.

(B) Structures of SM and its simulants (S1–S5).

2008, 2016; Cao et al., 2009; Xue et al., 2012) and have found applications in chemistry (Ke et al., 2013; Li et al., 2014, 2015; Li, 2014; Zhang et al., 2018, 2020; Guo et al., 2018; Kaizerman-Kane et al., 2019), biomedicine (Joseph et al., 2016; Chang et al., 2014; Duan et al., 2013; Li et al., 2017; Zhu et al., 2019; Chen et al., 2019; Si et al., 2015), and materials science (Strutt et al., 2012; Tan et al., 2014; Wang et al., 2016, 2018; Sun et al., 2018; Muhammed et al., 2019; Jie et al., 2018a, 2018b; Song et al., 2018; Ogoshi et al., 2015; Li et al., 2019; Zhou et al., 2019). Host-guest complexation in solution and in the solid state, as well as capture of SM simulants vapor, were comprehensively investigated. Particularly, the captured SM simulants by EtP5α cannot be released for at least 6 months.

Recently, the adsorption and photocatalytic oxidation of SM simulants by MOFs have been well demonstrated (Ma et al., 2019; Cao et al., 2019; Lee et al., 2020; Giannakoudakis and Bandosz, 2020). The present system based on organic macrocycles has the following characteristics (the advantages of pillar[5]arene over MOF are summarized in Table S1): (1) easy accessibility: EtP5 can be prepared through a single-step reaction in high yield of more than 70%, and all reagents are cheap and commercially available; (2) good stability: crystalline materials of EtP5 are stable to moisture; (3) high complexation ability and adsorption stability: SM and its simulants can be quantitatively prisoned in pillar[5]arene containers for quite a long time; (4) convenient modification: mono-, di-, tetra-, and per-substituted pillar[5]arenes can be conveniently obtained. These characteristics would make the present capture of SM find potential applications in degradation and protection materials.

RESULTS

Host-Guest Binding in Solution

Caution

SM is a reactive alkylating and cytotoxic agent. The experiments of host-guest complexation studies were carefully carried out in a fume hood with adequate protection by experienced personnel (more details see Transparent Methods in the Supplemental Information).

First, ^{1}H NMR studies were used to investigate host-guest binding behavior of EtP5 and SM in solution. Figure 2 shows the ^{1}H NMR spectra of SM that were obtained in the absence and presence of one equivalent (eq.) of EtP5 in o-xylene-d_{10}. Proton H_b gives a very large upfield shift of -0.42 ppm and H_a shows so remarkable broadening that its signal could not be observed. At the same time, protons $H_{1,3,4}$ of EtP5 exhibit downfield shifts ($\Delta\delta = 0.26$–0.30 ppm) as a consequence of de-shielding effects. These observations indicate an unambiguous binding event.

Five SM simulants, S1–S5 (Figure 1), were also examined as guest molecules in order to systematically study host-guest inclusion behavior. Among these simulants, 2-chloroethyl ethyl sulfide (S1), known as "half
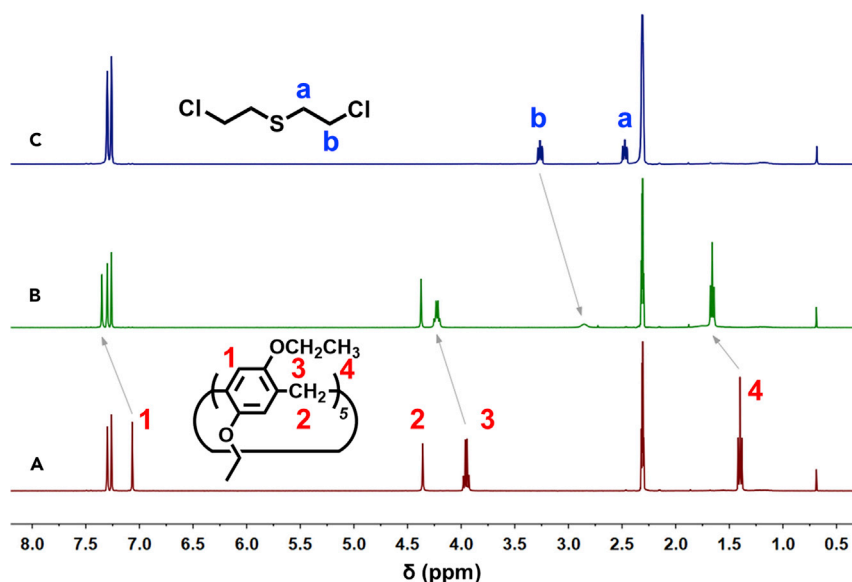
Figure 2. ^{1}H NMR Spectra (400 MHz, 298 K, D_2O) at 5.0 mM in *o*-xylene-d_{10}

(A) EtP5.

(B) SM + EtP5.

(C) SM.

mustard," is also poisonous. S2 and S4 have similar structures to SM, with the middle S atom of SM changed to O and CH_2, respectively. S3 and S5 are monofunctional analogs of S2 and S4. Upon addition of EtP5, the guest protons appear similar to NMR changes, i.e., remarkable upfield shifts and broadening (Figures S1–S5), supporting the formation of host-guest complexes. For comparison purpose, the interaction between *per*-ethylated pillar[6]arene (EtP6) and S2 was also evaluated. No obvious complexation was detected (Figure S6), which is reasonable that the guest is too small in comparison with EtP6's cavity.

The binding events were further validated by two-dimensional nuclear Overhauser effect spectroscopy (2D NOESY) experiments. From the NOESY spectra of S1@EtP5, strong correlations were observed between all the guest protons $H_{a–d}$ and the aromatic protons (H_1) and ethyl protons (H_3) of the host (Figure S7). Similarly, the NOESY spectra of S2@EtP5 exhibited unequivocal correlation peaks between the methylene protons $H_{a,b}$ of S2 and the aromatic protons (H_1) and ethyl protons (H_3) of EtP5 (Figure S8).

Association constants (K_a) of certain host-guest pairs were determined by employing ^{1}H NMR titration methods (Table 1 and Figure S9). A molar ratio plot for EtP5 and SM based on ^{1}H NMR data indicates 1:1 binding stoichiometry (Figure S10). The K_a value of EtP5 toward SM [$(6.2 \pm 0.6) \times 10^3$ M^{-1}] is 4.8 times larger than that for S2 [$(1.3 \pm 0.1) \times 10^3$ M^{-1}], yet it is 2.9 times lower than that for S4 [$(1.8 \pm 0.3) \times 10^4$ M^{-1}]. The middle methylene of the S4@EtP5 complex can mediate additional C–H$\cdots\pi$ interactions, resulting in strong host-guest interactions. The binding affinities of SM, S2, and S4 containing two Cl atoms were found to be significantly greater than those for their monofunctional analogs, S1, S3, and S5 (Table 1). This is because the cooperative hydrogen bonds and dispersion forces between the two ends of the guest and the two cavity portals of the macrocycle enhance the host-guest binding affinity.

Crystallographic Investigations

Five host-guest crystal structures of SM simulants, S1@EtP5, S2@EtP5, S3@EtP5, S4@EtP5 and S5@EtP5, and particularly, an X-ray crystal of the real chemical warfare agent, SM@EtP5, were successfully obtained. Details of the crystals are summarized in Table S2. As shown in Figure 3A–3F, the guests are encapsulated at the center of the EtP5 cavity, forming the 1:1 host-guest complexes. In the crystal structure of SM@EtP5 (Figure 3A), there are four C–H$\cdots\pi$ interactions between the methylenes of SM and the benzenes of EtP5, with C–H$\cdots$ring distances of 2.72–3.01 Å (Figure 3G). Only one of the end chlorines forms five C–H$\cdots$Cl hydrogen bonds with the host portal ethyls (Figure 3H), thereby suggesting that SM is a bit longer compared with the host height. This observation is consistent with our previously reported result that linear

Host	Guest	K_a (M^{-1})[a]
EtP5	SM	$(6.2 \pm 0.6) \times 10^3$
EtP5	S1	$(2.9 \pm 0.3) \times 10^2$
EtP5	S2	$(1.3 \pm 0.1) \times 10^3$
EtP5	S3	67 ± 6
EtP5	S4	$(1.8 \pm 0.3) \times 10^4$
EtP5	S5	$(7.9 \pm 0.6) \times 10^2$
EtP6	S2	[b]

Table 1. Association Constants (K_a) Corresponding to Interactions between SM and Its Simulants with EtP5

[a]K_a values were determined in o-xylene-d_{10} by using ^{1}H NMR titration methods.
[b]Host-guest complexation was not observed.

ditopic guests with four methylene (–CH$_2$–) linkers are suitable axles for pillar[5]arenes (Li et al., 2010). C–H$\cdots$S hydrogen bonds were also observed between the ethyls of EtP5 and the sulfur atom of the guest (Figure 3I). More interestingly, there exist triple sulfur–arene interactions between the S atom of SM and the benzenes of EtP5, with S$\cdots$ring distances of 3.95–4.50 Å (Figure 3J) (Meyer et al., 2003). In the crystal structures of S1–S5@EtP5 (Figures 3B–3F), guests are encapsulated in the center of the EtP5 cavity by C–H$\cdots\pi$/Cl/S interactions for S1@EtP5 (Figure S11A), C–H$\cdots$O/Cl interactions for S2@EtP5 (Figure S11B), C–H$\cdots\pi$/Cl/O interactions for S3@EtP5 (Figure S11C), and C–H$\cdots\pi$/Cl interactions for S4@EtP5 and S5@EtP5 (Figures S11D and S11E). These results indicated the formation of inclusion complexes with high stabilities in the solid state, where multiple C–H$\cdots\pi$ and hydrogen bonding interactions are dominant driving forces.

Vapor Adsorption

Based on the above binding investigation in solution and in the solid state, we wonder whether we can realize the adsorption of SM and its simulants by pillararene-based crystalline materials (EtP5α) (Figure S12). Previously, Ogoshi and Huang et al. (Ogoshi et al., 2015; Jie et al., 2018a, 2018b) reported the adsorption and separation behavior of crystalline pillar[n]arenes. This novel class of materials was termed as nonporous adaptive crystals (NACs) (Jie et al., 2018a, 2018b). Very recently, NACs of other macrocycles such as biphen[n]arene (Wang et al., 2019), hybrid[3]arene (Zhou et al., 2020), leaning towerarene (Wu et al., 2020), geminiarene (Wu and Yang, 2019), and tiararenes (Yang et al., 2020) have also been reported, showing interesting adsorption and separation properties. Notice that, in our vapor adsorption tests, SM simulants were utilized because no effective protection was available during the experiments for testing the real SM.

Figure 4 shows the time-dependent solid-vapor sorption results of EtP5α toward SM simulants. The uptake amount of S1–S5 in EtP5α increased over time. It was found that the similar adsorption amount of each simulant was observed at equilibrium with the guest/host ratio reaching 1.0–1.2/1 eq. according to ^{1}H NMR results (Figures S13–S17), indicating SM simulants are contained in the bulk of EtP5α crystals. Thermogravimetric analysis (TGA) measurements further confirmed the quantitative adsorption (Figure S18). EtP5α showed no apparent weight loss after heating to 200°C, demonstrating its stability (Figure S18A). Meanwhile, S1@EtP5 had a mass loss of 12.4% below 200°C. The weight loss was calculated to be 1.0 S1 molecule per EtP5 molecule (mol/EtP5), which is typical for the vapor adsorption results. Intriguingly, we found that the adsorbed guest molecules could not be released by EtP5α upon exposing in air at room temperature for at least 6 months (Figures 4F and S19–S23), indicating the activated crystal materials of EtP5α have ultrastable containment ability for SM simulants. What's more, SM simulants could be totally removed under vacuum at 80°C (Figure S24). There was no loss of uptake capacity of EtP5α for adsorption of SM simulants after multiple cycles (Figure S25). In addition, the energies of interactions for the complexes of SM@EtP5 and S1@EtP5 in the crystal state were calculated by molecular mechanics calculations (details in Supplemental Information). The calculated binding energy between EtP5 and SM was 144.6 kJ mol^{-1}, which is higher than that for S1@EtP5 (125.7 kJ mol^{-1}). These results are in accord with the complexation selectivity in solution.
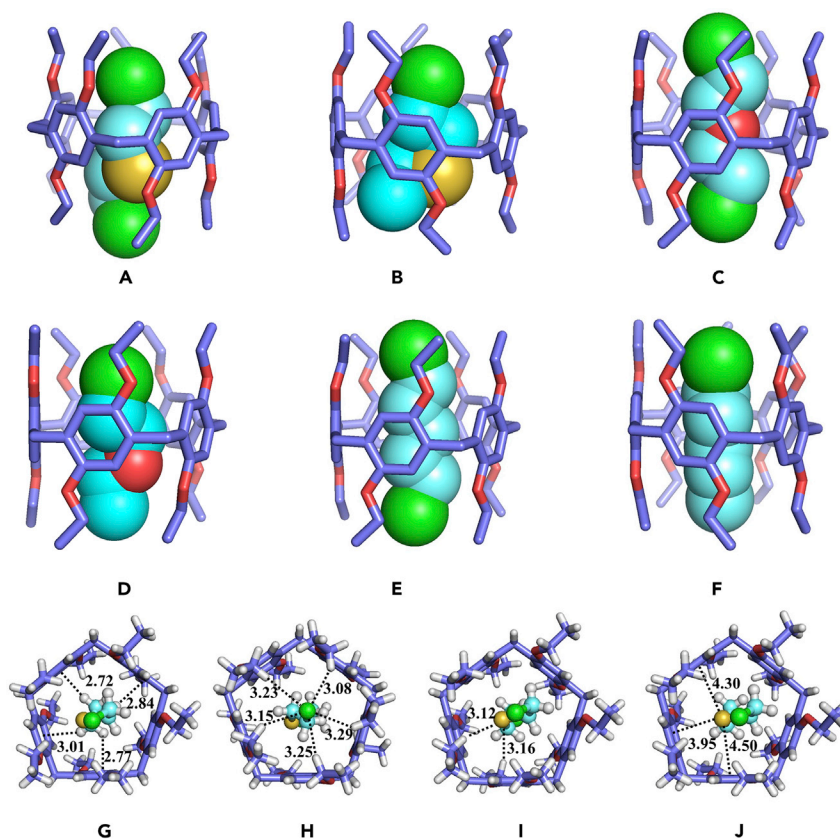
Figure 3. Single Crystal Structures of Host-Guest Complexes

(A) SM@EtP5. (B) S1@EtP5. (C) S2@EtP5. (D) S3@EtP5. (E) S4@EtP5. (F) S5@EtP5. Chlorine is shown in green, sulfur is shown in yellow, and oxygen is shown in red. Noncovalent bonding parameters of SM@EtP5: Hydrogen bond distances (Å) of C–H⋯π (G), C–H⋯Cl (H), C–H⋯S (I), and S⋯π (J). See Figure S11 and Table S2 and Data S1.

In order to investigate the mechanism upon uptake of SM simulants vapor by EtP5α (Figure 5G), powder X-ray diffraction (PXRD) experiments were carried out. The PXRD patterns of EtP5α after adsorption of SM simulants were completely different from the pattern for EtP5α (Figure 5H) (Figure S26), indicating that the capture of SM simulants induces the structural transformation of the host crystals. Meanwhile, the PXRD patterns of EtP5α after adsorption of SM simulants were almost the same with each other as well as are in good agreement with that simulated from S1–S5@EtP5 crystals (Figures 5I–5M and S26), suggesting that nonporous adaptive crystals of EtP5α transform to the same structure from EtP5α to S1–S5@EtP5. As can be seen from Figures 5B–5F, each EtP5 molecule was perpendicular to form herringbone structure with a body-to-window packing mode in S1–S5@EtP5, which is different from the SM@EtP5 with a window-to-window packing mode (Figure 5A). In addition, it is noted that the structure of S1@EtP5 could transform back to the original structure of EtP5α by removal of S1 under vacuum at 80°C after 12 h (Figure S27).

DISCUSSION

In summary, we have demonstrated efficient containment of SM and its simulants by pillar[5]arene, which is the first example of strong interactions of SM by macrocyclic receptors. ^{1}H NMR, 2D NOESY, and X-ray single crystal analysis show that strong binding events occur not only in solution but also in the solid state, which are driven by multiple C–H⋯π/Cl/S/O hydrogen bonding interactions. In addition, adaptive EtP5α crystals can be a great adsorbent to efficiently and quantitatively adsorb SM simulants with the guest-induced solid-state crystal structure transformation and the captured SM simulants could be contained in the materials for at least half a year. Considering the easy and cheap accessibility, convenient modification, and effective adsorption properties of pillar[5]arenes, the interesting encapsulation of SM
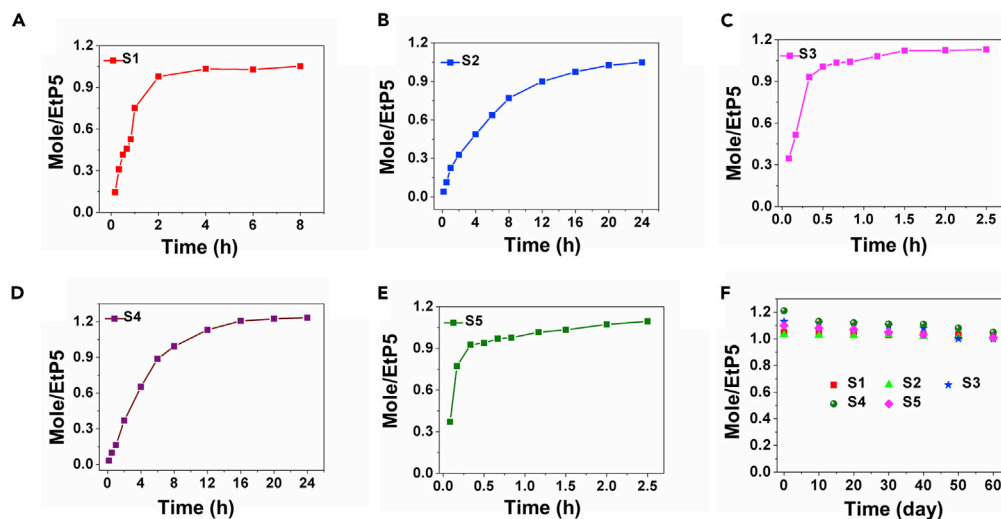
Figure 4. Time-Dependent Vapor Sorption Plot of SM Simulants Vapor by EtP5α at 25°C
(A) S1.
(B) S2.
(C) S3.
(D) S4.
(E) S5.
(F) Recorded residual guest/host ratio of adsorbed S1–S5 vapor by EtP5α after exposure in air for 6 months.

holds great potential for the sensing, detoxification, and protection materials for this chemical warfare agent. Endeavors to explore these possibilities are currently underway.

Limitations of the Study

As an effective protective material, crystalline ethylated pillar[5]arene cannot be used for degradation of sulfur mustard. Further investigations would focus on detoxifying mustard gas by functionalized pillar[5]arene. In addition, the TGA experiment for SM complex and the vapor adsorption test for SM were not determined owing to no effective protection for the highly toxic SM.

Resource Availability

Lead Contact

Further information and requests for resources and reagents should be directed to and will be fulfilled by the Lead Contact, Chunju Li (cjli@shu.edu.cn)

Materials Availability

This study did not generate new unique reagents.

Data and Code Availability

All data needed to evaluate the conclusions in the paper are present in the paper and/or the Supplemental Information. Additional data related to this paper may be requested from the authors. Supplementary crystallographic data for this paper can be obtained free of charge from the Cambridge Crystallographic Data Centre via www.ccdc.cam.ac.uk/data_request/cif. CCDC numbers are 1831237, 1884850, 1831239, 1884851, 1831240, and 1884852, respectively.

METHODS

All methods can be found in the accompanying Transparent Methods supplemental file.

SUPPLEMENTAL INFORMATION

Supplemental Information can be found online at https://doi.org/10.1016/j.isci.2020.101443.
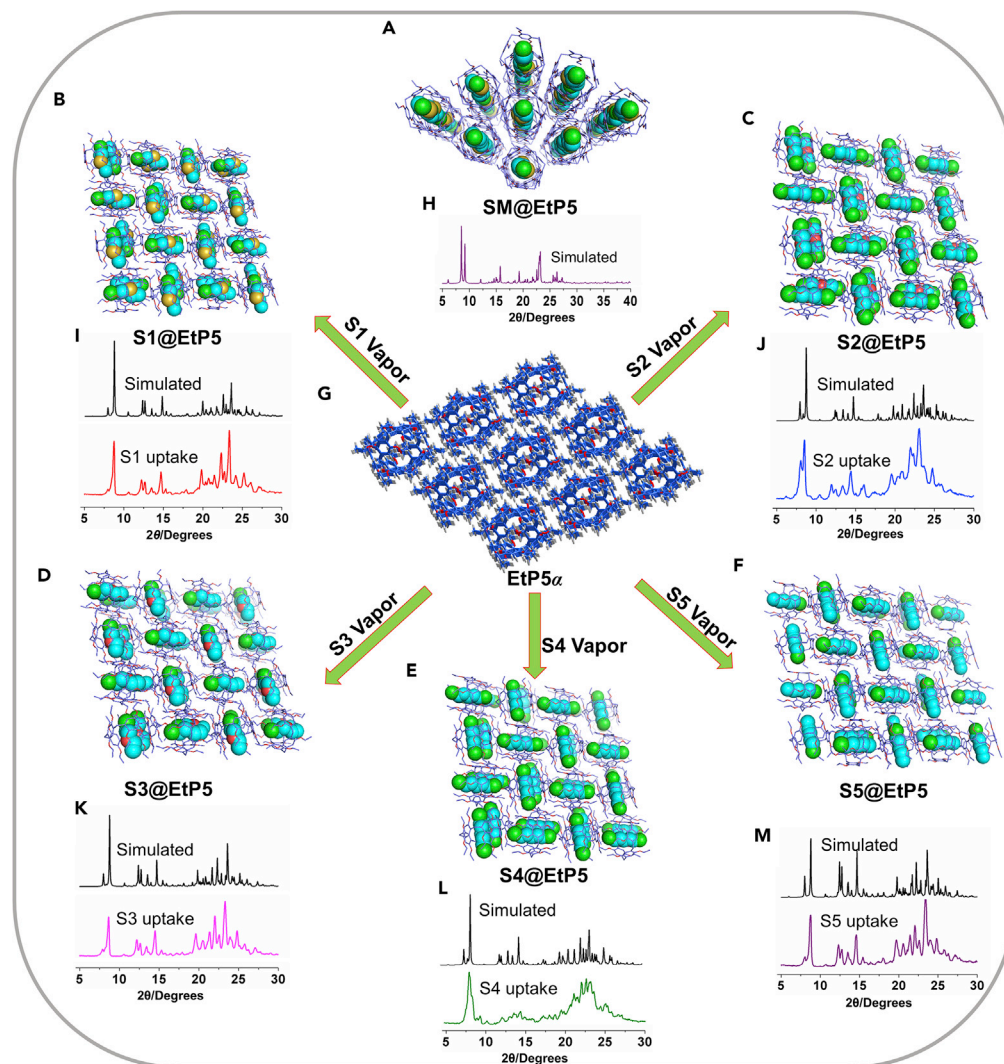
Figure 5. Crystal Packing Structures and PXRD Patterns

(A–F) Crystal structures of (A) SM@EtP5, (B) S1@EtP5, (C) S2@EtP5, (D) S3@EtP5, (E) S4@EtP5, and (F) S5@EtP5.

(G) The structure of EtP5α (Jie et al., 2018a, 2018b).

(H) Simulated PXRD pattern from the single crystal structure of SM@EtP5.

(I–M) The comparisons of PXRD patterns. Top: simulated PXRD patterns from single crystal structure of S1–S5@EtP5; bottom: PXRD patterns of EtP5α after uptake of S1–S5 vapor.

AUTHOR CONTRIBUTIONS

C.L. and Q.M. excogitated this project and designed the experiments. B.L. performed most experiments and wrote the original manuscript. C.L., Q.M. and B.L. supervised the project and revised this paper. S.L., B.W., Z.M., and Y.W. carried out part of the experiments. All authors discussed and commented on the manuscript.

DECLARATION OF INTERESTS

The authors declare no competing interests.

REFERENCES

Ajami, D., and Rebek, J. (2013). Chemical approaches for detection and destruction of nerve agents. Org. Biomol. Chem. 11, 3936–3942.

Alsbaiee, A., Smith, B.J., Xiao, L., Ling, Y., Helbling, D.E., and Dichtel, W.R. (2016). Rapid removal of organic micropollutants from water by a porous β-cyclodextrin polymer. Nature 529, 190–194.

Bobbitt, N.S., Mendonca, M.L., Howarth, A.J., Islamoglu, T., Hupp, J.T., Farha, O.K., and Snurr, R.Q. (2017). Metal–organic frameworks for the removal of toxic industrial chemicals and chemical warfare agents. Chem. Soc. Rev. 46, 3357–3385.

Cao, D., Kou, Y., Liang, J., Chen, Z., Wang, L., and Meier, H. (2009). A facile and efficient preparation of pillararenes and a pillarquinone. Angew. Chem. Int. Ed. 48, 9721–9723.

Cao, M., Pang, R., Wang, Q.-Y., Han, Z., Wang, Z.-Y., Dong, X.-Y., Li, S.-F., Zang, S.-Q., and Mak, T.C.W. (2019). Porphyrinic silver cluster assembled material for simultaneous capture and photocatalysis of mustard-gas simulant. J. Am. Chem. Soc. 141, 14505–14509.

Chang, Y., Yang, K., Wei, P., Huang, S., Pei, Y., Zhao, W., and Pei, Z. (2014). Cationic vesicles based on amphiphilic pillar[5]arene capped with ferrocenium: a redox-responsive system for drug/siRNA co-delivery. Angew. Chem. Int. Ed. 53, 13126–13346.

Chen, S., Ruan, Y., Brown, J.D., Gallucci, J., Maslak, V., Hadad, C.M., and Badjić, J.D. (2013). Assembly of amphiphilic baskets into stimuli-responsive vesicles. developing a strategy for the detection of organophosphorus chemical nerve agents. J. Am. Chem. Soc. 135, 14964–14967.

Chen, J., Ni, H., Meng, Z., Wang, J., Huang, X., Dong, Y., Sun, C., Zhang, Y., Cui, L., Li, J., et al. (2019). Supramolecular trap for catching polyamines in cells as an anti-tumor strategy. Nat. Commun. 10, 3546.

Decoste, J.B., and Peterson, G.W. (2014). Metal–organic frameworks for air purification of toxic chemicals. Chem. Rev. 114, 5695–5727.

Duan, Q., Cao, Y., Li, Y., Hu, X., Xiao, T., Lin, C., Pan, Y., and Wang, L. (2013). pH-responsive supramolecular vesicles based on water-soluble pillar[6]arene and ferrocene derivative for drug delivery. J. Am. Chem. Soc. 135, 10542–10549.

Evison, D., Hinsley, D., and Rice, P. (2001). Chemical weapons. BMJ 324, 332–335.

Fruton, J.S., Stein, W.H., Stahmann, M.A., and Golumbic, C. (1946). Chemical reactions of the nitrogen mustard gases.[1] VI. the reactions of the

nitrogen mustard gases with chemical compounds of biological interest. J. Org. Chem. 11, 571–580.

Giannakoudakis, D.A., and Bandosz, T.J. (2020). Defectous UiO-66 MOF nanocomposites as reactive media of superior protection against toxic vapors. ACS Appl. Mater. Interfaces 12, 14678–14689.

Guo, M., Wang, X., Zhan, C., Demay-Drouhard, P., Li, W., Du, K., Olson, M.A., Zuilhof, H., and Sue, A.C.-H. (2018). Rim-differentiated C5-symmetric tiara-pillar[5]arenes. J. Am. Chem. Soc. 140, 74–77.

Islamoglu, T., Chen, Z., Wasson, M.C., Buru, C.a.T., Kirlikovali, K.O., Afrin, U., Mian, M.R., and Farha, O.K. (2020). Metal-organic frameworks against toxic chemicals. Chem. Rev. https://doi.org/10.1021/acs.chemrev.9b00828.

Jang, Y.J., Kim, K., Tsay, O.G., Atwood, D.A., and Churchill, D.G. (2015). Destruction and detection of chemical warfare agents. Chem. Rev. 115, PR1–PR76.

Jie, K., Zhou, Y., Li, E., and Huang, F. (2018a). Nonporous adaptive crystals of pillararenes. Acc. Chem. Res. 51, 2064–2072.

Jie, K., Liu, M., Zhou, Y., Little, M.A., Pulido, A., Chong, S.Y., Stephenson, A., Hughes, A.R., Sakakibara, F., Ogoshi, T., et al. (2018b). Near-ideal xylene selectivity in adaptive molecular pillar[n]arene crystals. J. Am. Chem. Soc. 140, 6921–6930.

Joseph, R., Naugolny, A., Feldman, M., Herzog, I.M., Fridman, M., and Cohen, Y. (2016). Cationic pillararenes potently inhibit biofilm formation without affecting bacterial growth and viability. J. Am. Chem. Soc. 138, 754–757.

Kaizerman-Kane, D., Hadar, M., Tal, N., Dobrovetsky, R., Zafrani, Y., and Cohen, Y. (2019). pH-Responsive pillar[6]arene-based water-soluble supramolecular hexagonal boxes. Angew. Chem. Int. Ed. 58, 5302–5306.

Ke, C., Strutt, N.L., Li, H., Hou, X., Hartlieb, K.J., McGonigal, P.R., Ma, Z., Iehl, J., Stern, C.L., Cheng, C., et al. (2013). Pillar[5]arene as a co-factor in templating rotaxane formation. J. Am. Chem. Soc. 135, 17019–17030.

Kim, S.K., Lim, J.M., Pradhan, T., Jung, H.S., Lynch, V.M., Kim, J.S., Kim, D., and Sessler, J.L. (2014). Self-association and nitroaromatic-induced deaggregation of pyrene substituted pyridine amides. J. Am. Chem. Soc. 136, 495–505.

Kumar, V., and Anslyn, E.V. (2013). A selective turn-on fluorescent sensor for sulfur mustard simulants. J. Am. Chem. Soc. 135, 6338–6344.

Lee, D.T., Jamir, J.D., Peterson, G.W., and Parsons, G.N. (2020). Protective fabrics: metal organic framework textiles for rapid photocatalytic sulfur mustard simulant detoxification. Matter 2, 404–415.

Li, C. (2014). Pillararene-based supramolecular polymers: from molecular recognition to polymeric aggregates. Chem. Commun. 50, 12420–12433.

Li, C., Xu, Q., Li, J., Yao, F., and Jia, X. (2010). Complex interactions of pillar[5]arene with paraquats and bis(pyridinium) derivatives. Org. Biomol. Chem. 8, 1568–1576.

Li, Z.-Y., Zhang, Y., Zhang, C.-W., Chen, L.-J., Wang, C., Tan, H., Yu, Y., Li, X., and Yang, H.-B. (2014). Cross-linked supramolecular polymer gels constructed from discrete multi-pillar[5]arene metallacycles and their multiple stimuli-responsive behavior. J. Am. Chem. Soc. 136, 8577–8589.

Li, S.-H., Zhang, H.-Y., Xu, X., and Liu, Y. (2015). Mechanically selflocked chiral gemini-catenanes. Nat. Commun. 6, 7590.

Li, B., Meng, Z., Li, Q., Huang, X., Kang, Z., Dong, H., Chen, J., Sun, J., Dong, Y., Li, J., et al. (2017). A pH responsive complexation-based drug delivery system for oxaliplatin. Chem. Sci. 8, 4458–4464.

Li, E., Zhou, Y., Zhao, R., Jie, K., and Huang, F. (2019). Dihalobenzene shape sorting by nonporous adaptive crystals of perbromoethylated pillararenes. Angew. Chem. Int. Ed. 58, 3981–3985.

Liu, Y., Howarth, A.J., Vermeulen, N.A., Moon, S.-Y., Hupp, J.T., and Farha, O.K. (2017). Catalytic degradation of chemical warfare agents and their simulants by metal-organic frameworks. Coordin Chem. Rev. 346, 101–111.

Ma, K., Islamoglu, T., Chen, Z., Li, P., Wasson, M.C., Chen, Y., Wang, Y., Peterson, G.W., Xin, J.H., and Farha, O.K. (2019). Scalable and template-free aqueous synthesis of zirconium-based metal−organic framework coating on textile fiber. J. Am. Chem. Soc. 141, 15626–15633.

Mei, L., Li, F., Lan, J.-H., Wang, C., Xu, C., Deng, H., Wu, Q., Hu, K., Wang, L., Chai, Z., et al. (2019). Anion-adaptive crystalline cationic material for $^{99}TcO_4^-$ trapping. Nat. Commun. 10, 1532.

Meyer, E.A., Castellano, R.K., and Diederich, F. (2003). Interactions with aromatic rings in chemical and biological recognition. Angew. Chem. Int. Ed. 42, 1210–1250.

Muhammed, M.A.H., Cruz, L.K., Emwas, A.-H., ElZohry, A.M., Moosa, B., Mohammed, O.F., and Khashab, N.M. (2019). Pillar[5]arene-stabilized

silver nanoclusters: extraordinary stability and luminescence enhancement induced by host–guest interactions. Angew. Chem. Int. Ed. *58*, 15665–15670.

Ogoshi, T., Kanai, S., Fujinami, S., Yamagishi, T.-a., and Nakamoto, Y. (2008). *para*-Bridged symmetrical pillar[5]arenes: their lewis acid catalyzed synthesis and host–guest property. J. Am. Chem. Soc. *130*, 5022–5023.

Ogoshi, T., Sueto, R., Yoshikoshi, K., Sakata, Y., Akine, S., and Yamagishi, T. (2015). Host–guest complexation of perethylated pillar[5]arene with alkanes in the crystal state. Angew. Chem. Int. Ed. *54*, 9849–9852.

Ogoshi, T., Yamagishi, T.-a., and Nakamoto, Y. (2016). Pillar-shaped macrocyclic hosts pillar[n]arenes: new key players for supramolecular chemistry. Chem. Rev. *116*, 7937–8002.

Schneider, C., Bierwisch, A., Koller, M., Worek, F., and Kubik, S. (2016). Detoxification of VX and other V-type nerve agents in water at 37°C and pH 7.4 by substituted sulfonatocalix[4]arenes. Angew. Chem. Int. Ed. *55*, 12668–12672.

Shah, M.S., Tsapatsis, M., and Siepmann, J.I. (2017). Hydrogen sulfide capture: from absorption in polar liquids to oxide, zeolite, and metal−organic framework adsorbents and membranes. Chem. Rev. *117*, 9755–9803.

Si, W., Xin, P., Li, Z.-T., and Hou, J.-L. (2015). Tubular unimolecular transmembrane channels: construction strategy and transport activities. Acc. Chem. Res. *48*, 1612–1619.

Song, N., Kakuta, T., Yamagishi, T.-a., Yang, Y.-W., and Ogoshi, T. (2018). Molecular-scale porous materials based on pillar[n]arenes. Chem *4*, 2029–2053.

Strutt, N.L., Fairen-Jimenez, D., Iehl, J., Lalonde, M.B., Snurr, R.Q., Farha, O.K., Hupp, J.T., and Stoddart, J.F. (2012). Incorporation of an A1/A2-difunctionalized pillar[5]arene into a metal–organic framework. J. Am. Chem. Soc. *134*, 17436–17439.

Sun, Y., Zhang, F., Quan, J., Zhu, F., Hong, W., Ma, J., Pang, H., Sun, Y., Tian, D., and Li, H. (2018). A biomimetic chiral-driven ionic gate constructed by pillar[6]arene-based host–guest systems. Nat. Commun. *9*, 2617.

Szinicz, L. (2005). History of chemical and biological warfare agents. Toxicology *214*, 167–181.

Tan, L.-L., Li, H., Tao, Y., Zhang, X.A., Wang, B., and Yang, Y.-W. (2014). Pillar[5]arene-based supramolecular organic frameworks for highly selective CO₂-capture at ambient conditions. Adv. Mater. *26*, 7027–7031.

Tchalala, M.R., Bhatt, P.M., Chappanda, K.N., Tavares, S.R., Adil, K., Belmabkhout, Y., Shkurenko, A., Cadiau, A., Heymans, N., De Weireld, G., et al. (2019). Fluorinated MOF platform for selective removal and sensing of SO₂ from flue gas and air. Nat. Commun. *10*, 1328.

Wang, K., Guo, D.-S., Zhang, H.-Q., Li, D., Zheng, X.-L., and Liu, Y. (2009). Highly effective binding of viologens by p-sulfonatocalixarenes for the treatment of viologen poisoning. J. Med. Chem. *52*, 6402–6412.

Wang, Q.-Q., Begum, R.A., Day, V.W., and Bowman-James, K. (2013). Chemical mustard containment using simple palladium pincer complexes: the influence of molecular walls. J. Am. Chem. Soc. *135*, 17193–17199.

Wang, Y., Ping, G., and Li, C. (2016). Efficient complexation between pillar[5]arenes and neutral guests: from host–guest chemistry to functional materials. Chem. Commun. *52*, 9858–9872.

Wang, S., Xu, Z., Wang, T., Xiao, T., Hu, X.-Y., Shen, Y.-Z., and Wang, L. (2018). Warm/cool-tone switchable thermochromic material for smart windows by orthogonally integrating properties of pillar[6]arene and ferrocene. Nat. Commun. *9*, 1737.

Wang, Y., Xu, K., Li, B., Cui, L., Li, J., Jia, X., Zhao, H., Fang, J., and Li, C. (2019). Efficient separation of *cis*- and *trans*-1,2-dichloroethene isomers by adaptive biphen[3]arene crystals. Angew. Chem. Int. Ed. *58*, 10281–10284.

Wattana, M., and Bey, T. (2009). Mustard gas or sulfur mustard: an old chemical agent as a new terrorist threat. Prehosp. Disast. Med. *24*, 19–29.

Wu, J.-R., and Yang, Y.-W. (2019). Geminiarene: molecular scale dual selectivity for chlorobenzene and chlorocyclohexane fractionation. J. Am. Chem. Soc. *141*, 12280–12287.

Wu, J.-R., Li, B., and Yang, Y.-W. (2020). Separation of bromoalkanes isomers by nonporous adaptive crystals of leaning pillar[6]arene. Angew. Chem. Int. Ed. *59*, 2251–2255.

Xue, M., Yang, Y., Chi, X., Zhang, Z., and Huang, F. (2012). Pillararenes, a new class of macrocycles for supramolecular chemistry. Acc. Chem. Res. *45*, 1294–1308.

Yang, W., Samanta, K., Wan, X., Thikekar, T.U., Chao, Y., Li, S., Du, K., Xu, J., Gao, Y., Zuilhof, H., and Sue, A.C.-H. (2020). Tiara[5]arenes: synthesis, solid-state conformational studies, host-guest properties, and application as nonporous adaptive crystals. Angew. Chem. Int. Ed. *59*, 2–8.

Yu, G., Zhou, X., Zhang, Z., Han, C., Mao, Z., Gao, C., and Huang, F. (2012). Pillar[6]arene/paraquat molecular recognition in water: high binding strength, pH-responsiveness, and application in controllable self-assembly, controlled release, and treatment of paraquat poisoning. J. Am. Chem. Soc. *134*, 19489–19497.

Zhang, H., Liu, Z., and Zhao, Y. (2018). Pillararene-based self-assembled amphiphiles. Chem. Soc. Rev. *47*, 5491–5528.

Zhang, X., Wang, X., Wang, B., Ding, Z.-J., and Li, C. (2020). Carbon-carbon double bond in pillar[5]arene cavity: selective binding of cis/trans-olefin isomers. Chin. Chem. Lett. https://doi.org/10.1016/j.cclet. 2020.02.037.

Zhou, Y., Jie, K., Zhao, R., Li, E., and Huang, F. (2019). Cyclic ether contaminant removal from water using nonporous adaptive pillararene crystals via host-guest complexation at the solid-solution interface. Research *2019*, 5406365.

Zhou, J., Yu, G., Li, Q., Wang, M., and Huang, F. (2020). Separation of benzene and cyclohexane by nonporous adaptive crystals of a hybrid[3]arene. J. Am. Chem. Soc. *142*, 2228–2232.

Zhu, H., Wang, H., Shi, B., Shangguan, L., Tong, W., Yu, G., Mao, Z., and Huang, F. (2019). Supramolecular peptide constructed by molecular Lego allowing programmable self-assembly for photodynamic therapy. Nat. Commun. *10*, 2412.

Supplemental Information

Capture of Sulfur Mustard by Pillar[5]arene:

From Host-Guest Complexation to Efficient

Adsorption Using Nonporous Adaptive Crystals

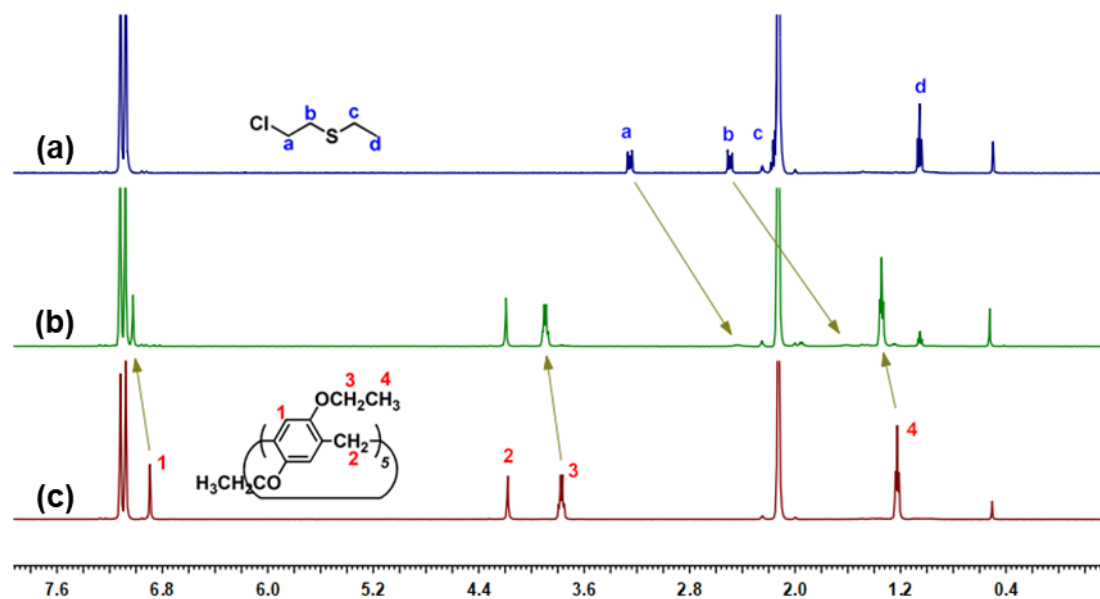Bin Li, Shuo Li, Bin Wang, Zhao Meng, Yongan Wang, Qingbin Meng, and Chunju Li

Figure S1. ^1H NMR spectra (*o*-xylene-d_{10}, 298 K, 500 MHz) of (a) S1, (b) S1 + EtP5, (c) EtP5 at 5.0–5.2 mM. Related to Figures 1 and 2.
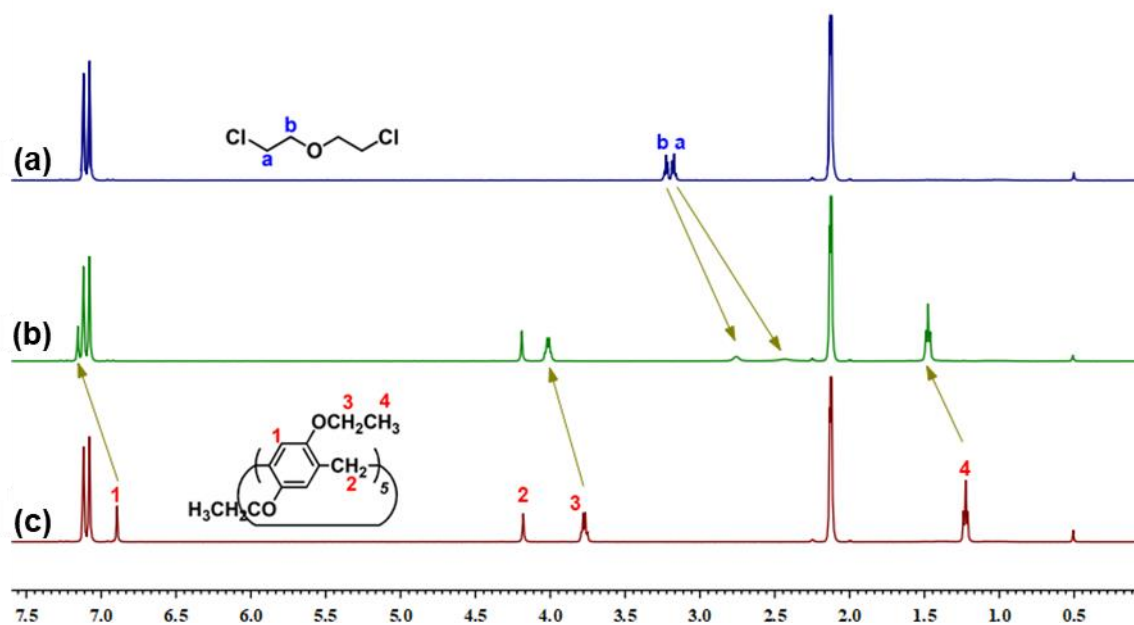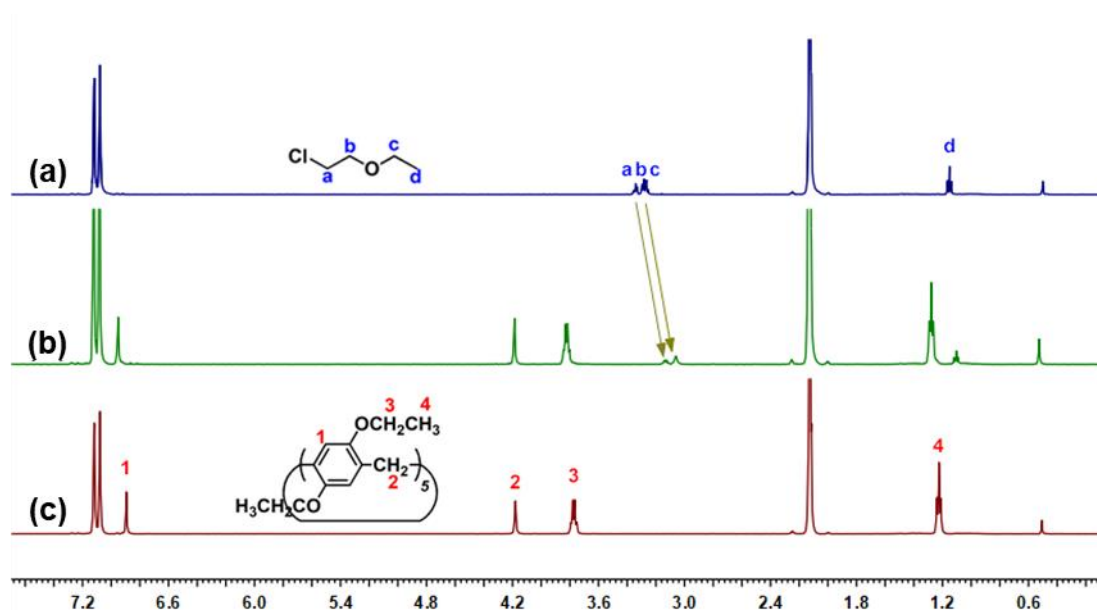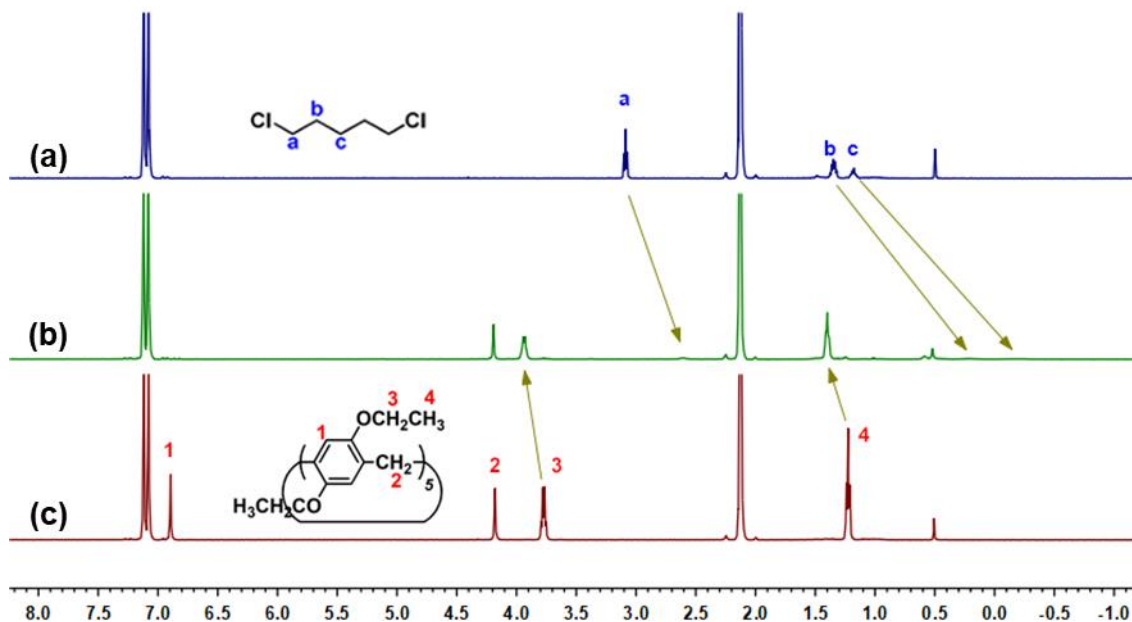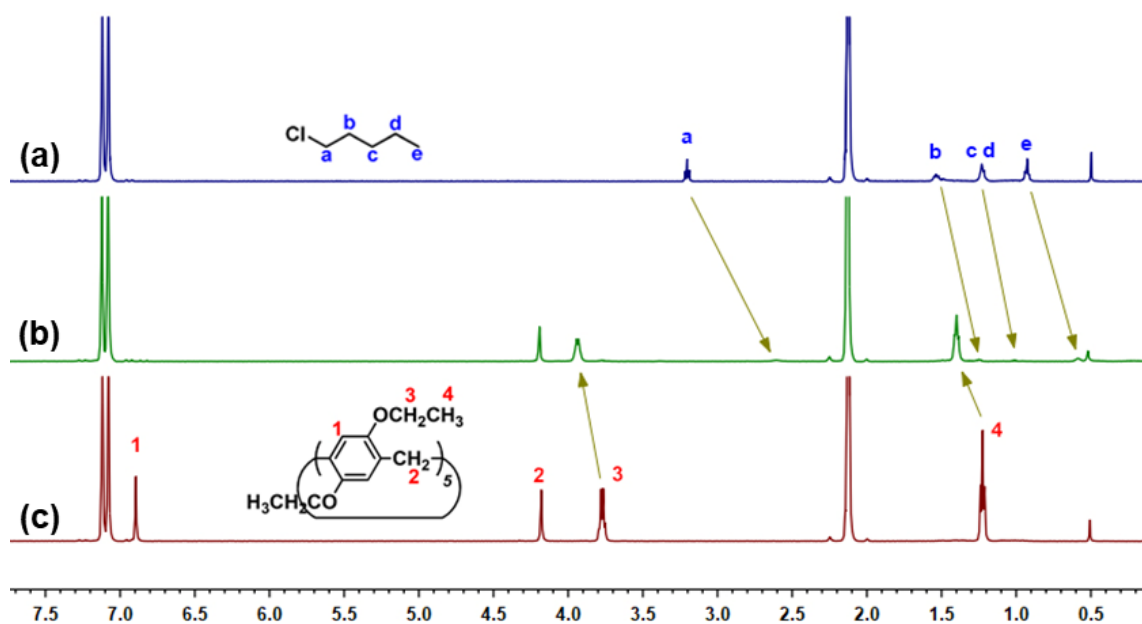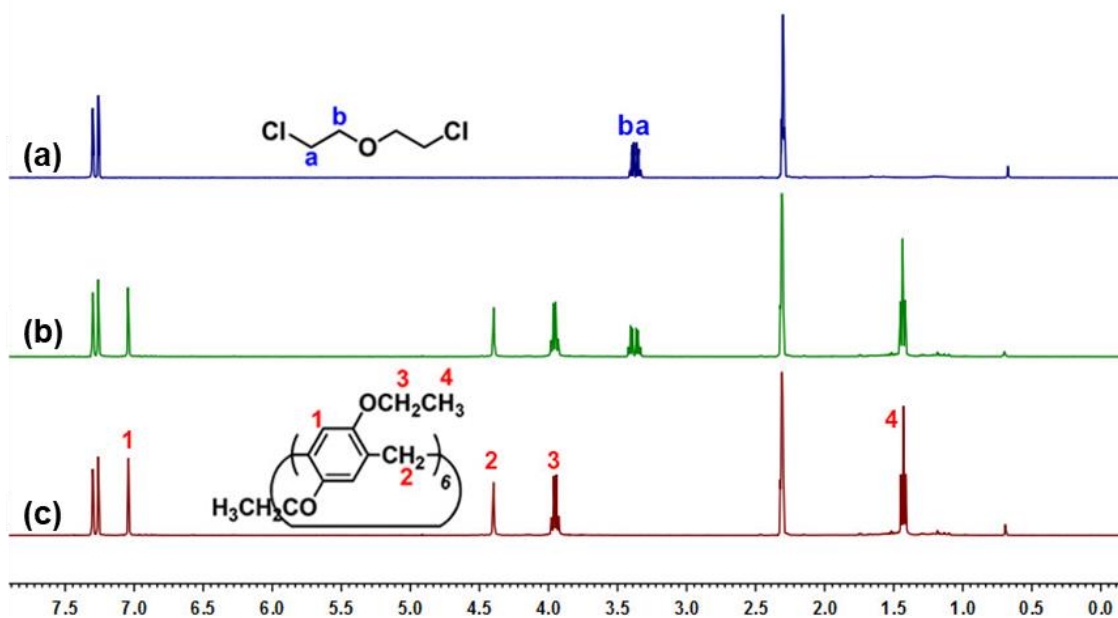

Figure S2. ^1H NMR spectra (*o*-xylene-d_{10}, 298 K, 500 MHz) of (a) S2, (b) S2 + EtP5, (c) EtP5 at 5.0–5.2 mM. Related to Figures 1 and 2.

Figure S3. ^{1}H NMR spectra (*o*-xylene-d_{10}, 298 K, 500 MHz) of (a) S3, (b) S3 + EtP5, (c) EtP5 at 5.0–5.1 mM. Related to Figures 1 and 2.

Figure S4. ^{1}H NMR spectra (*o*-xylene-d_{10}, 298 K, 500 MHz) of (a) S4, (b) S4 + EtP5, (c) EtP5 at 5.0–5.1 mM. Related to Figures 1 and 2.

Figure S5. ^{1}H NMR spectra (*o*-xylene-*d*$_{10}$, 298 K, 500 MHz) of (a) S5, (b) S5 + EtP5, (c) EtP5 at 4.9–5.1 mM. Related to Figures 1 and 2.

Figure S6. ^{1}H NMR spectra (*o*-xylene-*d*$_{10}$, 298 K, 500 MHz) of (a) S2, (b) S2 + EtP6, (c) EtP6 at 5.0–5.1 mM. Related to Figures 1 and 2.
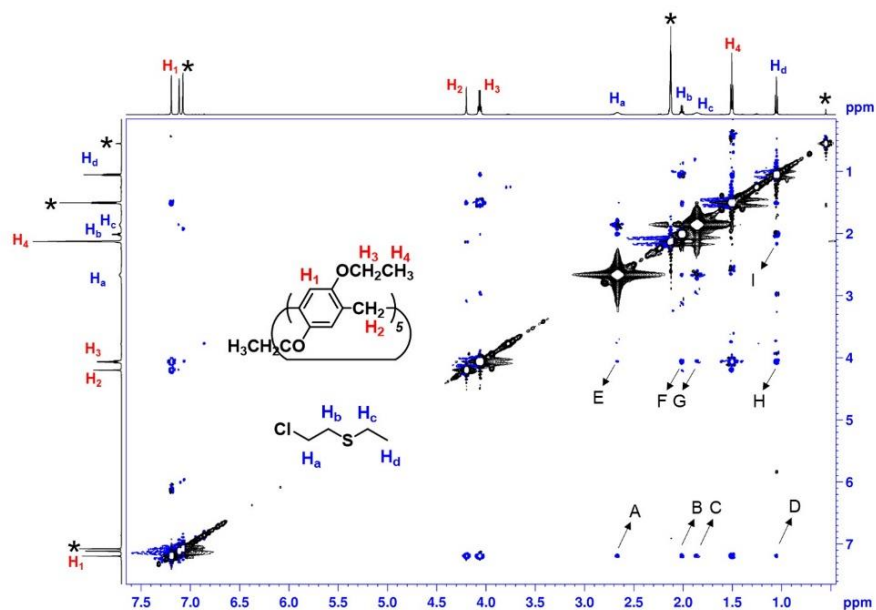
Figure S7. 2D NOESY (600 MHz, 298 K) analysis of S1 (15 mM) with EtP5 (45 mM) in *o*-xylene-*d*10 with a mixing time of 600 ms. Related to Figures 1 and 2.
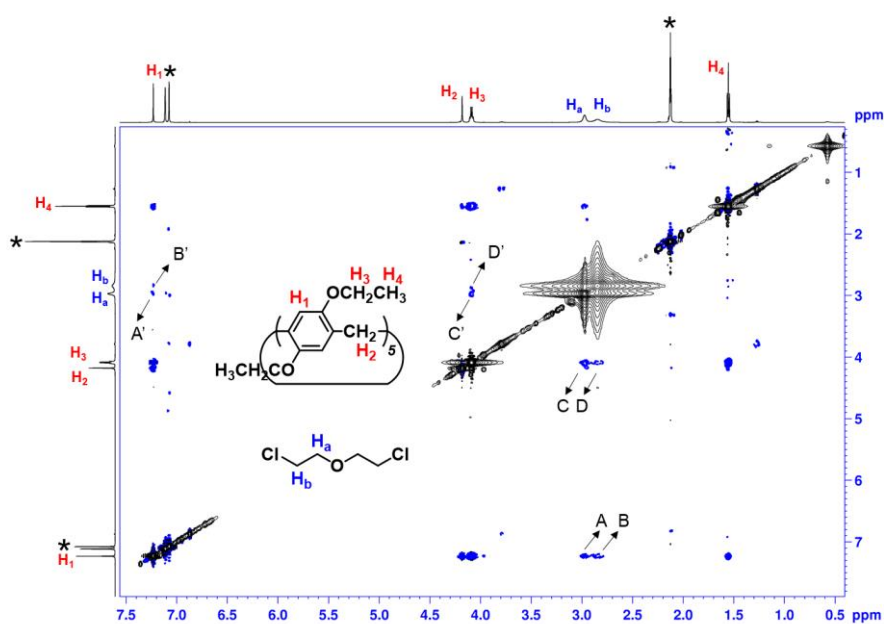
Figure S8. 2D NOESY (600 MHz, 298 K) analysis of S2 (15 mM) with EtP5 (45 mM) in *o*-xylene-*d*10 with a mixing time of 600 ms. Related to Figures 1 and 2.
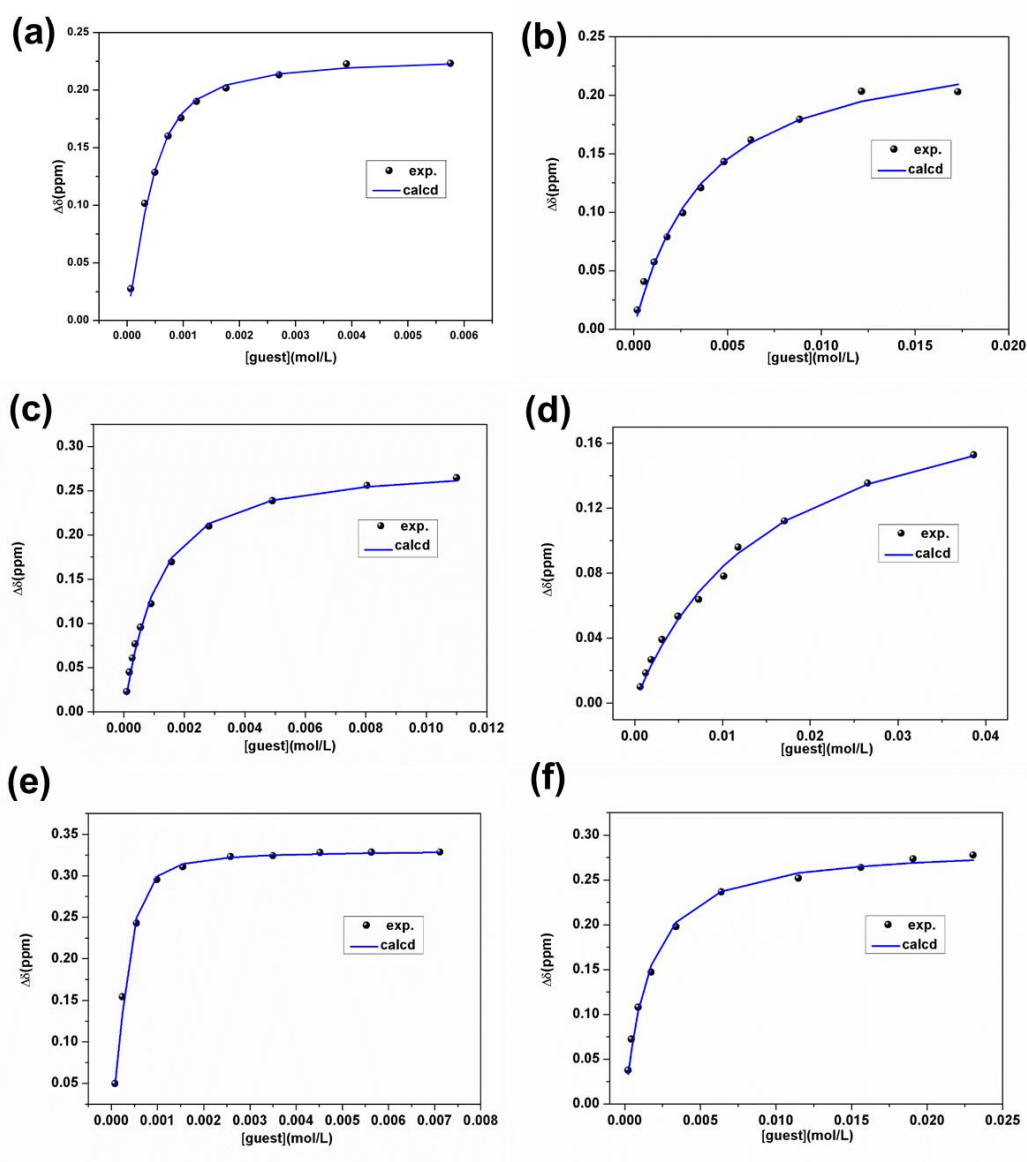
Figure S9. The non-linear curve-fitting for the complexation of EtP5 (0.5 mM) host with SM and its simulants in *o*-xylene-*d*$_{10}$ at 298 K. (a) The concentration of SM was 0, 0.06, 0.30, 0.50, 0.70, 1.0, 1.2, 1.8, 2.7, 3.9, 5.8 mM. (b) The concentration of S1 was 0.18, 0.55, 1.08, 1.78, 2.62, 3.59, 4.81, 6.25, 8.84, 12.15, 17.29 mM. (c) The concentration of S2 was 0.01, 0.19, 0.28, 0.37, 0.55, 0.90, 1.58, 2.81, 4.91, 8.04, 11.00 mM. (d) The concentration of S3 was 0.63, 1.26, 1.89, 3.12, 4.94, 7.30, 10.14, 11.80, 17.07, 26.56, 38.63 mM. (e) The concentration of S4 was 0.08, 0.24, 0.54, 0.99, 1.55, 2.58, 3.50, 4.52, 5.63, 7.11 mM. (f) The concentration of S5 was 0.22, 0.45, 0.89, 1.75, 3.89, 6.39, 11.48, 15.63, 19.08, 23.04 mM. Related to Figure 2 and Table 1.
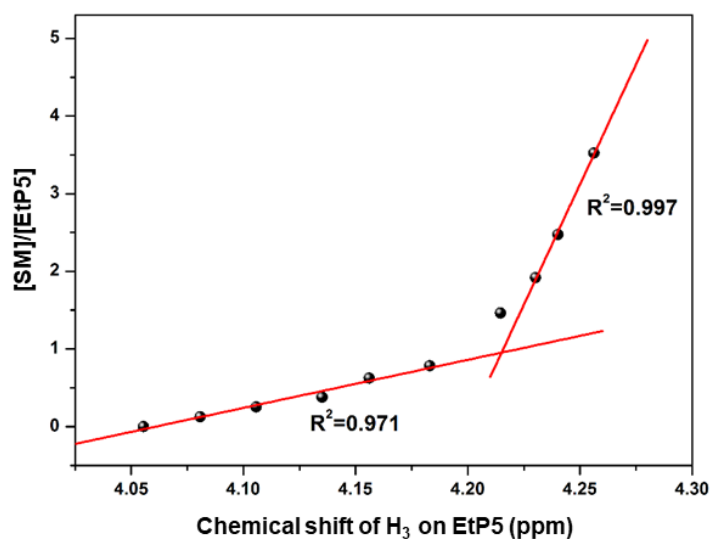
Figure S10. Mole ratio plot for EtP5 and SM from ^{1}H NMR (400 MHz, 298 K) experiments of EtP5 (with a fixed concentration) in *o*-xylene-d_{10} in the presence of different equivalents of SM, which indicates the 1 : 1 binding stoichiometry. Related to Figure 2.
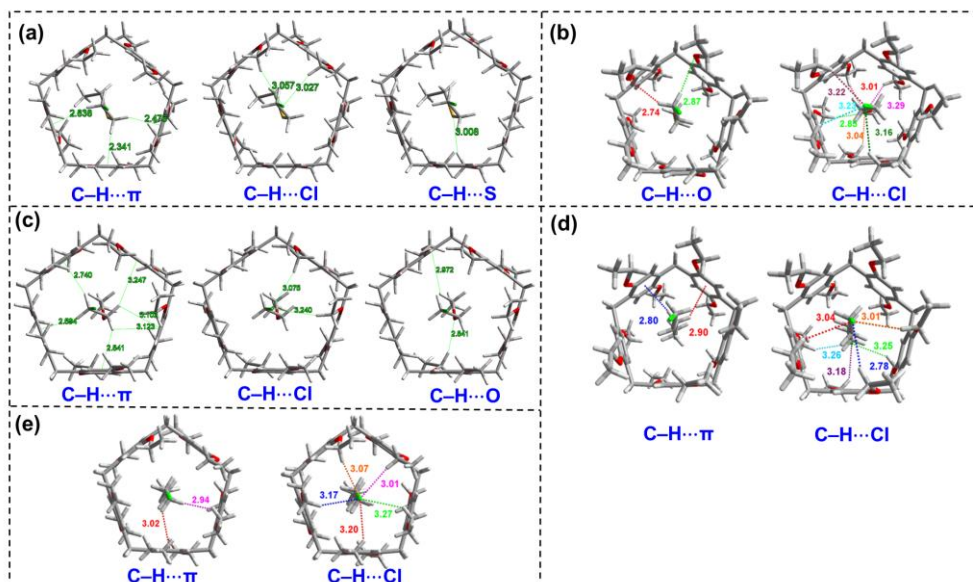

Figure S11. Hydrogen bonding parameters of S1–S5@EtP5. (a) S1@EtP5. (b) S2@EtP5. (c) S3@EtP5. (d) S4@EtP5. (e) S5@EtP5. Related to Figure 3.
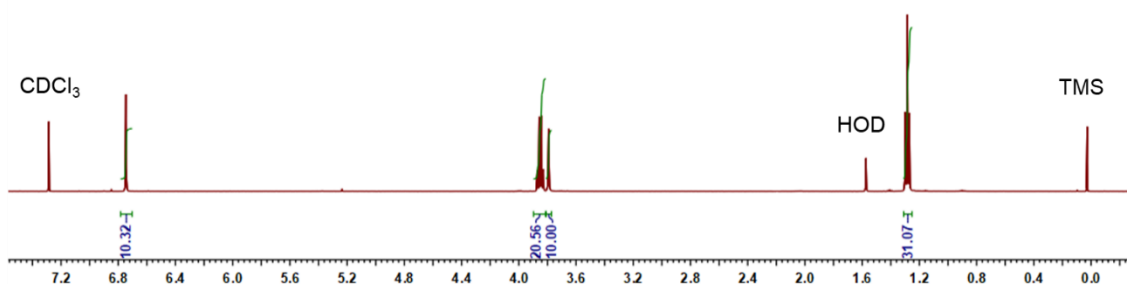
Figure S12. ^{1}H NMR spectrum (500 MHz) of activated crystals of EtP5 (EtP5α) in CDCl$_3$ at 298 K. Related to Figure 4.
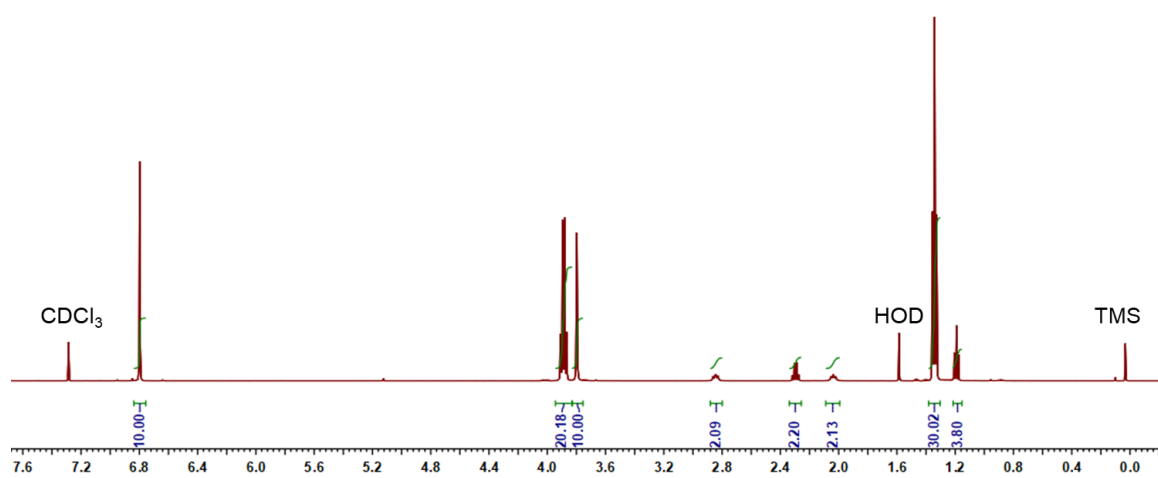

Figure S13. ^{1}H NMR spectrum (500 MHz) of EtP5α after capturing S1 for 4 hours in CDCl$_3$ at 298 K. Related to Figure 4.
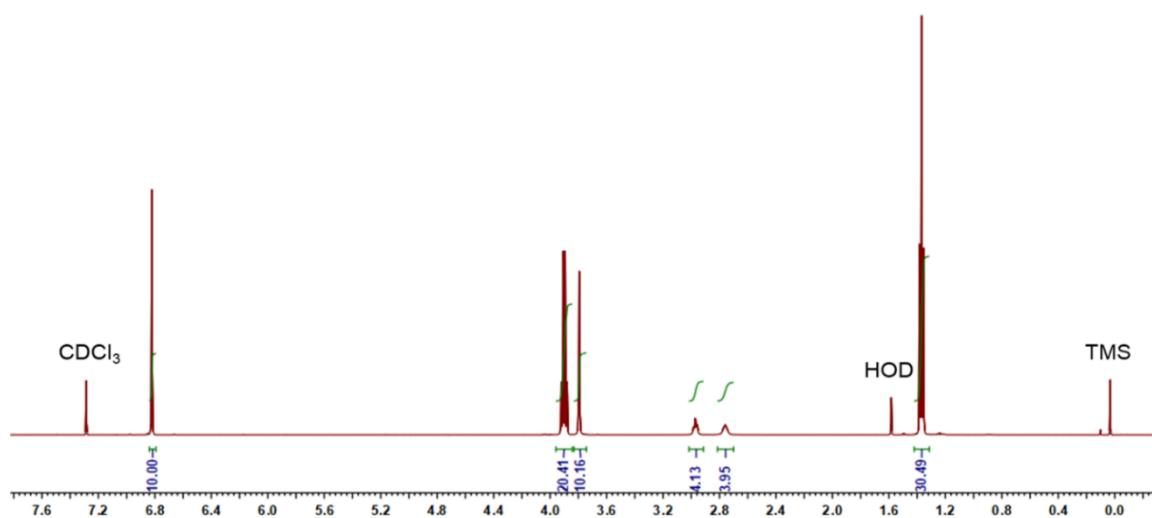
Figure S14. ^{1}H NMR spectrum (500 MHz) of EtP5α after capturing S2 for 16 hours in CDCl$_3$ at 298 K. Related to Figure 4.
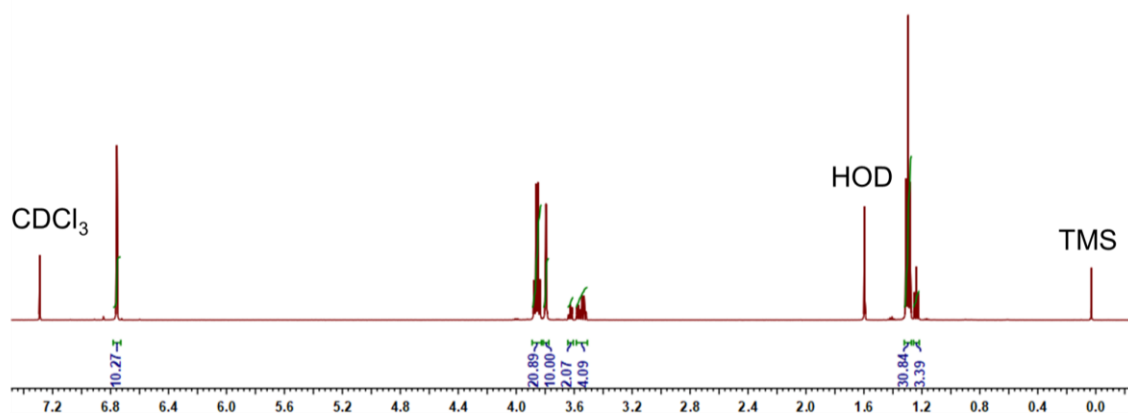

Figure S15. ^{1}H NMR spectrum (500 MHz) of EtP5α after capturing S3 for 2 hours in CDCl$_3$ at 298 K. Related to Figure 4.
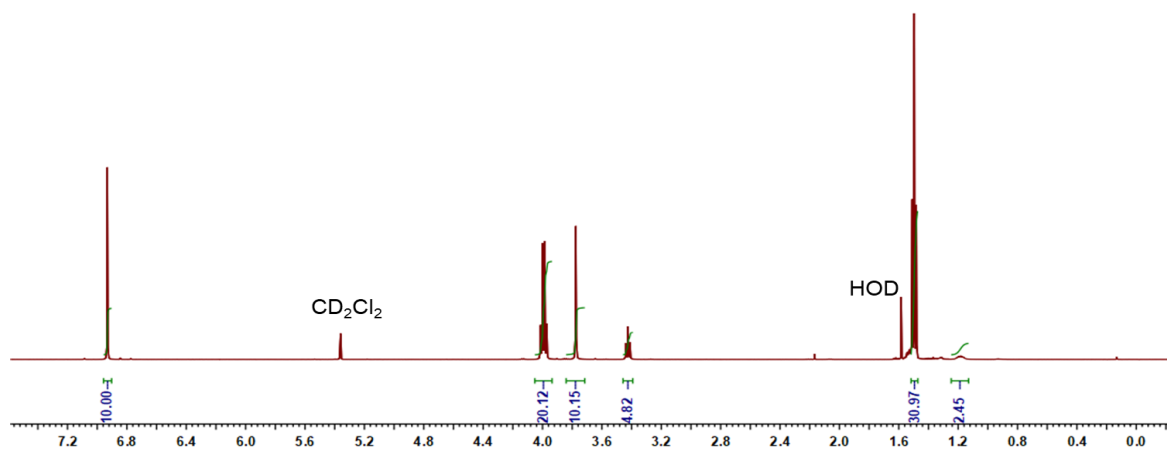
Figure S16. ^{1}H NMR spectrum (500 MHz) of EtP5α after capturing S4 for 16 hours in CD$_2$Cl$_2$ at 298 K. Related to Figure 4.
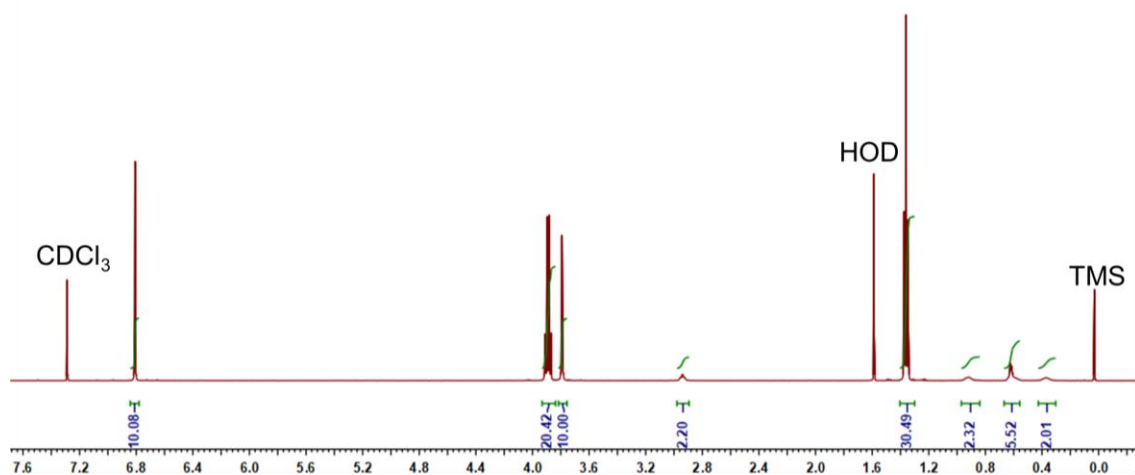

Figure S17. ^{1}H NMR spectrum (500 MHz) of EtP5α after capturing S5 for 2 hours in CD$_2$Cl$_2$ at 298 K. Related to Figure 4.
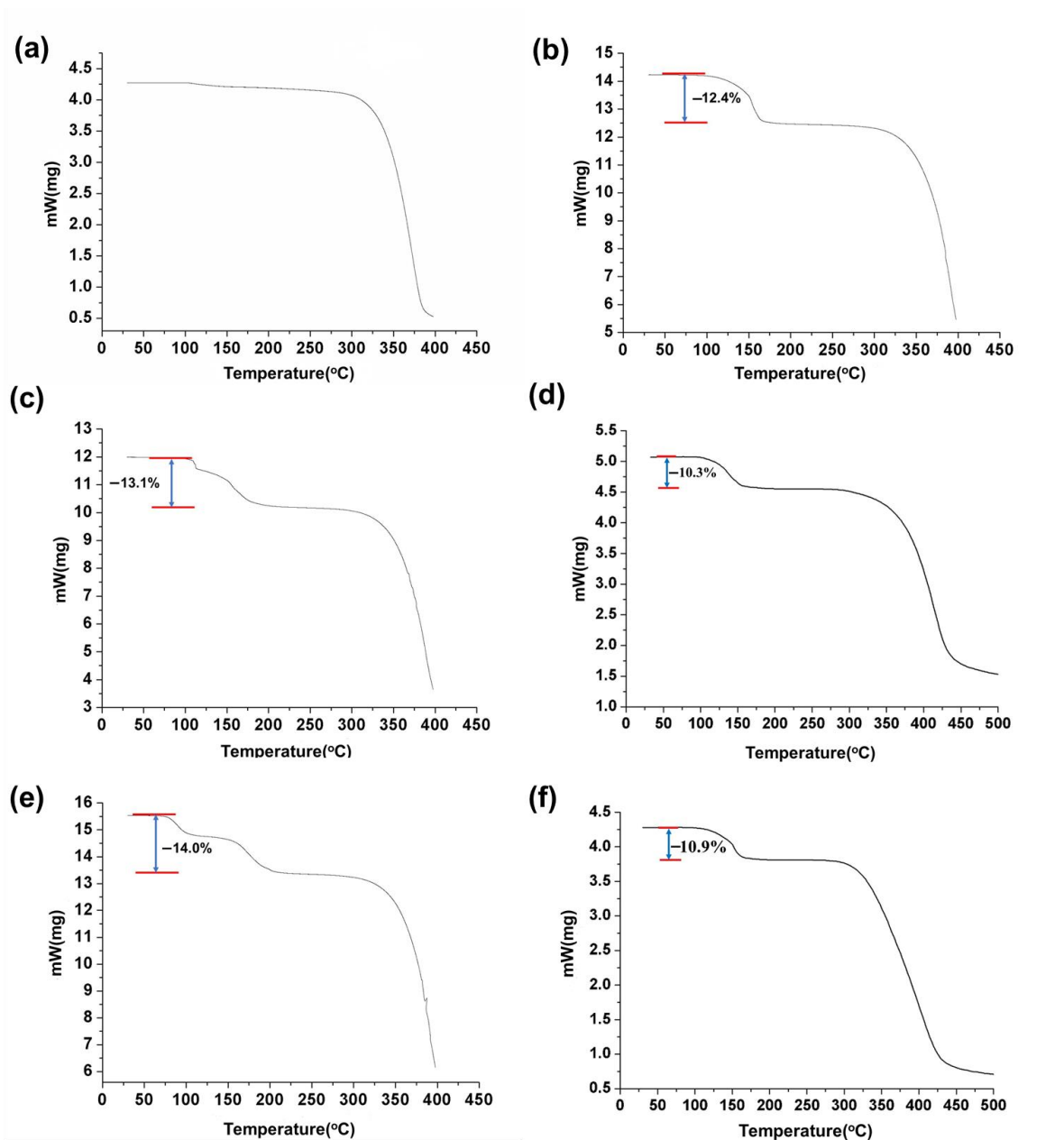
Figure S18. Thermogravimetric analysis of EtP5 before and after uptake of SM simulants. (a) EtP5α. EtP5α after adsorption of (b) S1, (c) S2, (d) S3, (e) S4 and (f) S5. Related to Figure 4.
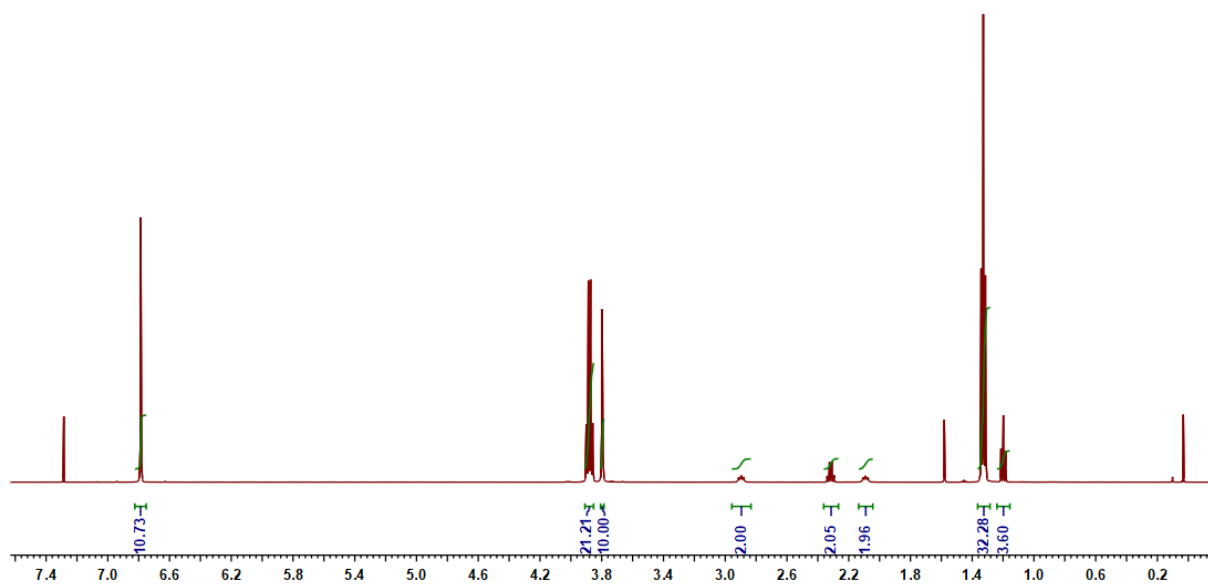
Figure S19. ^{1}H NMR (CDCl$_3$, 500 MHz, 298 K) spectrum of host-guest complex crystals EtP5 containing S1 after exposing to air for 6 months. Related to Figure 4.

Figure S20. ^{1}H NMR (CDCl$_3$, 500 MHz, 298 K) spectrum of host-guest complex crystals EtP5 containing S2 after exposing to air for 6 months. Related to Figure 4.

Figure S21. ¹H NMR (CDCl₃, 500 MHz, 298 K) spectrum of host-guest complex crystals EtP5 containing S3 after exposing to air for 6 months. Related to Figure 4.
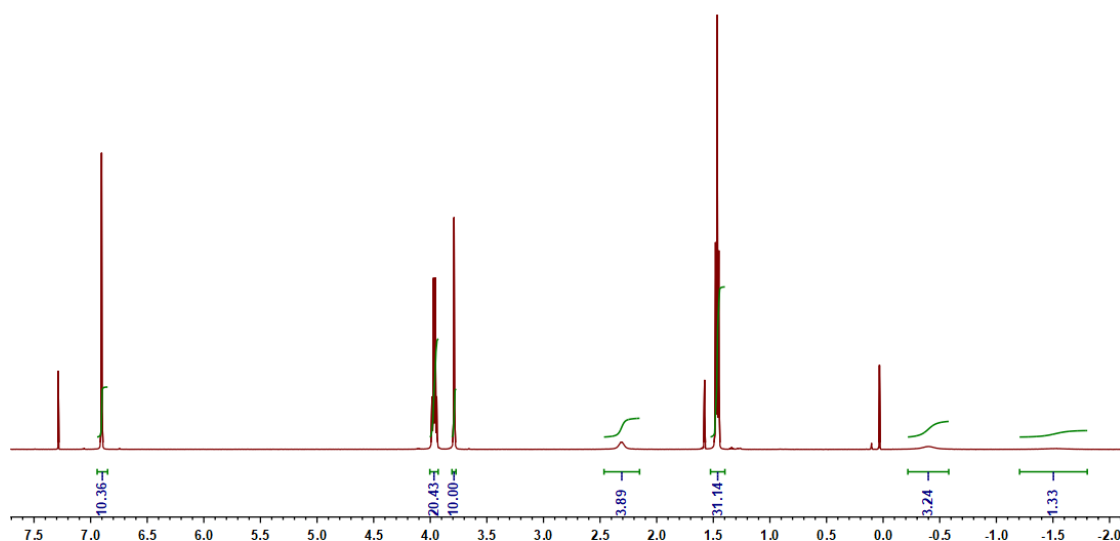
Figure S22. ¹H NMR (CDCl₃, 500 MHz, 298 K) spectrum of host-guest complex crystals EtP5 containing S4 after exposing to air for 6 months. Related to Figure 4.
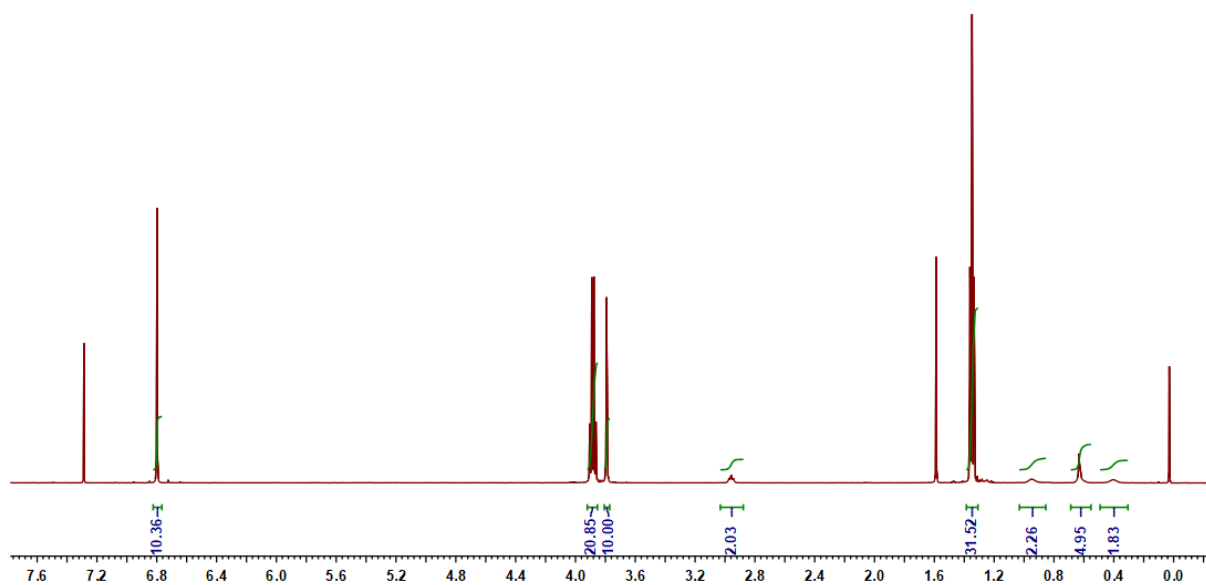
Figure S23. ¹H NMR (CDCl₃, 500 MHz, 298 K) spectrum of host-guest complex crystals EtP5 containing S5 after exposing to air for 6 months. Related to Figure 4.

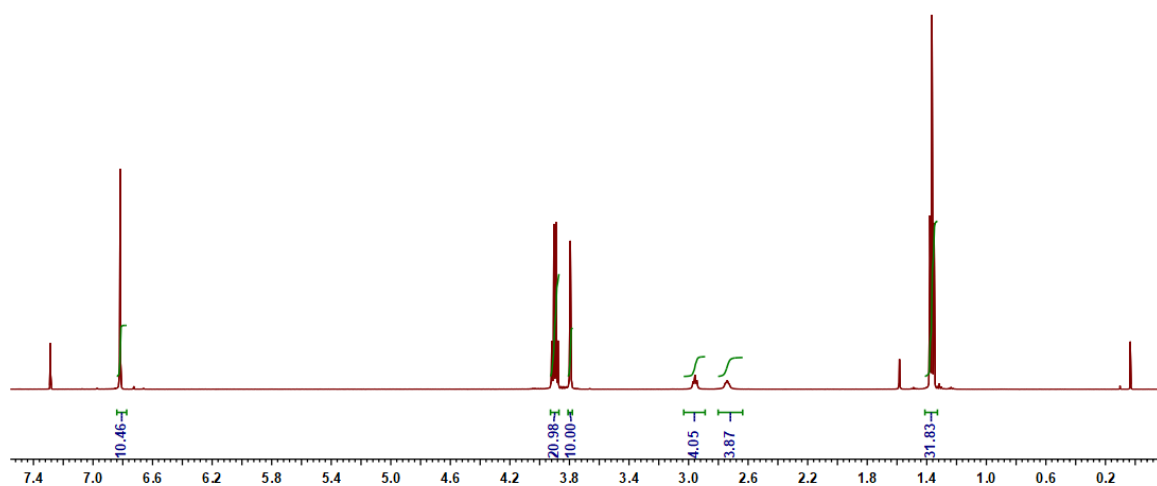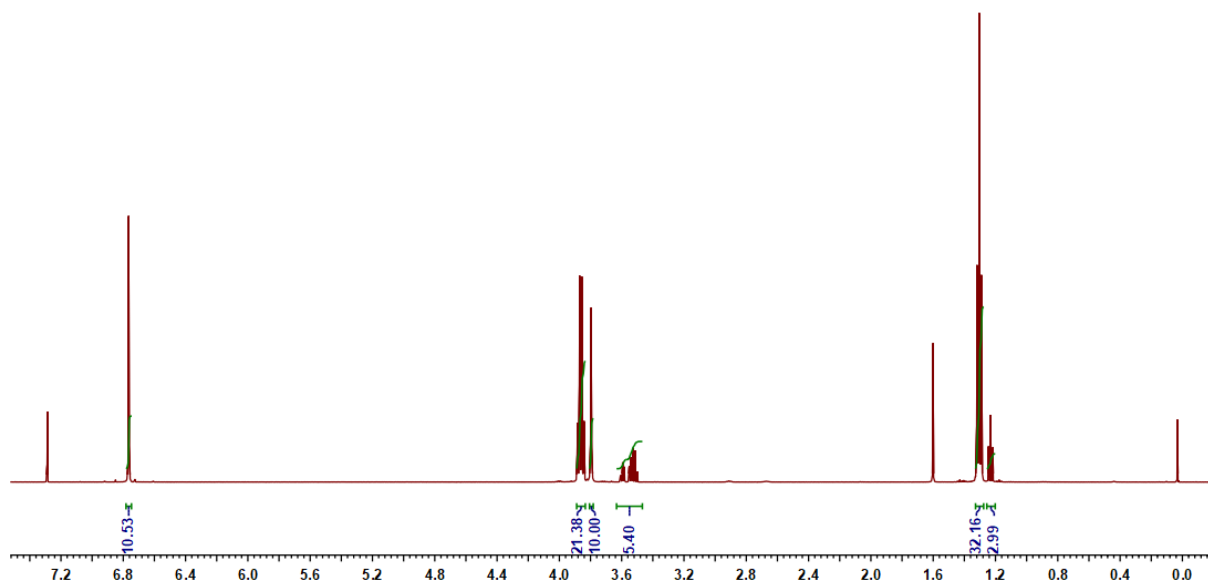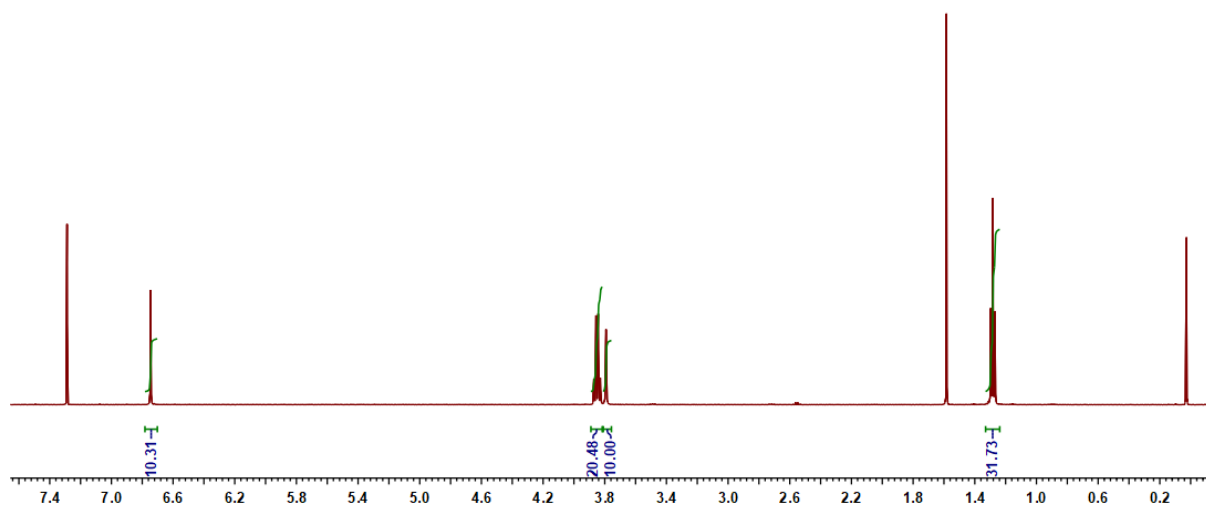**Figure S24.** ¹H NMR (CDCl₃, 500 MHz, 298 K) spectrum of EtP5 after desorption of S1. Related to Figure 4.
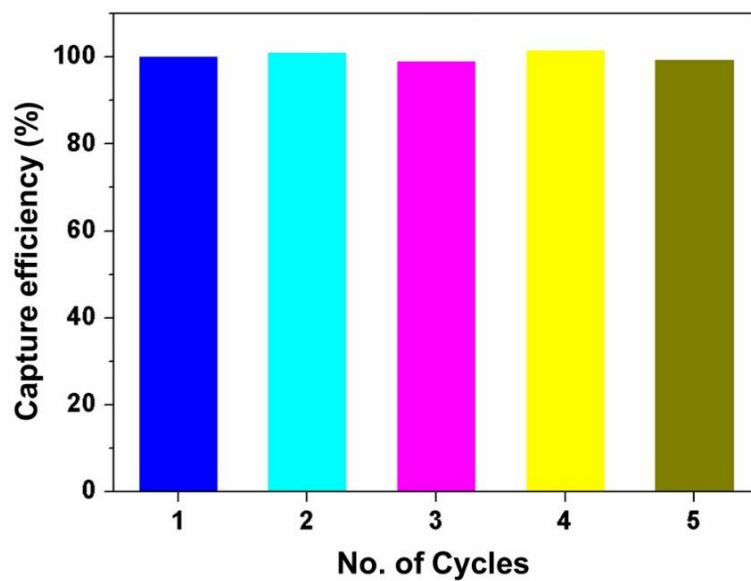
Figure S25. Cyclic S1 adsorption efficiency of EtP5α. Related to Figure 4.
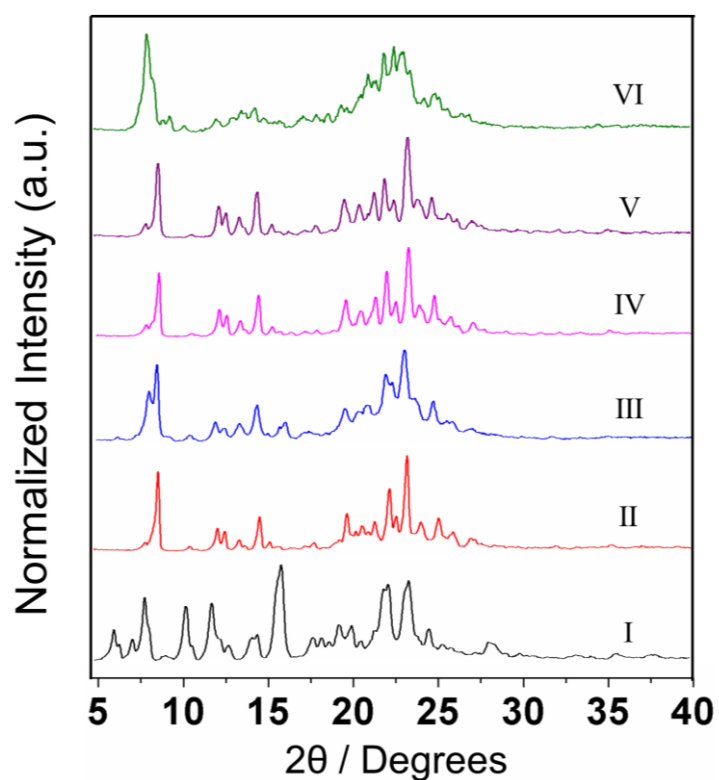
Figure S26. PXRD patterns of EtP5: (I) original EtP5α; after adsorption of S1 (II), S2 (III), S3 (IV), S4 (V) and S5 vapor, respectively. Related to Figure 5.
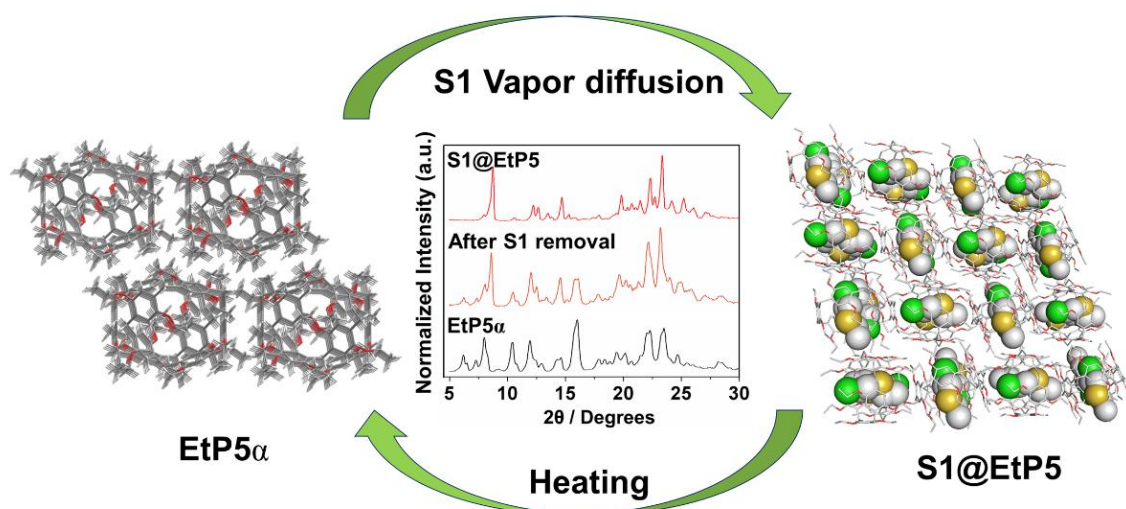
Figure S27. Structural representation of the transformation from EtP5α to S1@EtP5 upon uptake of S1 vapor and the release of S1 by heating. Insert: the PXRD of S2@EtP5 and after release of S1 guest upon heating. Related to Figures 4 and 5.

Table S1. Advantages of the pillar[5]arene over MOF. Related to Figure 1.

	Pillar[5]arene	MOF
Synthesis	Simple and cheap preparation on a large scale	Relatively difficult and expensive
Functionalization	Convenient modification	Relatively difficult post-modification
Stability	High chemical, and moisture stability	Sometimes low chemical, and/or moisture stability
Solubility	Soluble in common organic solvents	Barely soluble
Reusability	Good recyclability	Relatively poor regeneration ability

Table S2. Crystal data and structure refinement for SM@EtP5 and S1–S5@EtP5 complexes. Related to Figure 3 and Data S1.

	SM@EtP5	S1@EtP5	S2@EtP5	S3@EtP5	S4@EtP5	S5@EtP5
formula	$C_{59}H_{78}Cl_2O_{10}S$	$C_{59}H_{79}ClO_{10}S$	$C_{59}H_{78}Cl_2O_{11}$	$C_{59}H_{79}ClO_{11}$	$C_{60}H_{80}Cl_2O_{10}$	$C_{60}H_{81}ClO_{10}$
Mr [g mol^{-1}]	1050.17	1015.73	1034.11	999.67	1032.14	997.69
Temperature [K]	153(2)	170	113(2)	170(2)	153(2)	170.15
Wavelength [Å]	0.71073	1.34139	0.71073	1.34139	0.71073	1.34139
Crystal system	*Monoclinic*	*Orthorhombic*	*Orthorhombic*	*Orthorhombic*	*Orthorhombic*	*Orthorhombic*
Space group	P2$_1$/*n*	*Pbcn*	*Pbcn*	*Pbcn*	*Pbcn*	*Pbcn*
a [Å]	13.484(3)	41.973(3)	42.280(2)	42.4505(15)	42.325(9)	42.6501(16)
b [Å]	20.536(4)	15.9077(12)	15.7060(8)	15.8043(6)	15.891(3)	15.7339(6)
c [Å]	20.843(4)	16.8624(13)	16.8990(7)	16.6203(6)	17.004(3)	16.6216(6)
α [º]	90	90	90	90	90	90
β [º]	94.21(3)	90	90	90	90	90
γ [º]	90	90	90	90	90	90
V [Å^3]	5756(3)	11258.9(15)	11221.7(9)	11150.6(7)	11437(4)	11154.0(7)
Z	4	8	8	8	8	8
D$_{calcd}$ [g cm^{-3}]	1.212	1.198	1.224	1.191	1.199	1.188

μ [mm^{-1}]	0.204	0.910	0.174	0.694	0.169	0.684
F(000)	2248	4368	4432	4304	4432	4304
Crystal size [mm^3]	0.50×0.17×0.06	0.15×0.12×0.1	0.20×0.18×0.12	0.2×0.18×0.15	0.28×0.27×0.26	0.15×0.1×0.03
2θ range [º]	2.496–31.470	3.447–55.878	2.99–25.02	3.477–55.085	1.37–25.00	3.484–55.040
Reflections collected	66142	106897	62311	113630	64000	113529
Independent reflections, R_{int}	19005, 0.060	10733, 0.1020	9891, 0.0743	10624, 0.0679	10059, 0.0499	10625, 0.0888
Data/restraints/parameters	66142/0/678	10733/125/707	9891/0/659	10624/1610/707	10059/18/659	10632/1604/708
Goodness-of-fit on F^2	1.186	1.631	1.068	1.051	1.254	1.049
Final R_1 values (I> 2σ(I))	0.1377	0.1330	0.0608	0.0911	0.1279	0.0752
Final R_1 values (all data)	0.1895	0.1824	0.0965	0.1166	0.1324	0.1028
Final wR(F_2) values (all data)	0.3840	0.4501	0.1501	0.2814	0.3203	0.2187
Largest diff. peak and hole [e.Å^{-3}]	1.247/-0.799	0.725/-0.617	0.733/-0.467	0.830/-0.481	1.008/-1.065	0.64/-0.33
CCDC	1831237	1884850	1831239	1884851	1831240	1884852

Transparent Methods

Materials: Sulfur mustard was supplied by the Institute of Chemical Defense of Chinese People's Liberation Army, with purity higher than 96%. 2-Chloroethyl ethyl sulfide (S1), bis(2-chloroethyl) ether (S2), 2-chloroethyl ethyl ether (S3), 1,5-dichloropentane (S4) and 1-chloropentane (S5) were purchased from Adamas-beta Chemical Company.

Caution: SM is a highly toxic agent in nature. Therefore, in the associated experiments, handing of the micro-scale chemical agent should be performed only in a lab under well-ventilated fume hood by certified personnel. The operators should wear experimental gloves, applicable protective suit and mask and guarantee stringent protective measures to carry out the experiments carefully (Liu et al., 2016; Xu et al., 2014; Roy et al., 2012; Goud et al., 2014). After the completion of the experiment, SM need to be decontaminated by decontamination solution.

Synthesis of EtP5 and EtP6: The hosts of EtP5 and EtP6 were prepared according to the reported literature (Ogoshi et al., 2008; Hu et al., 2012). To the solution of 1,4-diethoxybenzene (12.0 g, 72 mmol) in chloroform (500 mL) was added paraformaldehyde (2.16 g, 72 mmol). The suspension was stirred at 25 °C for 30 min. And then, boron trifluoride diethyl etherate (9.0 ml, 72 mmol) was added to the solution. After continuing stirred at 25 °C for 20 min, the reaction was quenched by addition of water. The organic phase was separated and washed with saturated aqueous NaHCO$_3$, H$_2$O, and brine. The crude product was purified by column chromatograph to yield EtP5 (CH$_2$Cl$_2$/petroleum ether = 1:1, 2.56 g, 20 %) and EtP6 (CH$_2$Cl$_2$/petroleum ether = 4:1, 1.92 g, 15 %) as white solids.

Apparatus. ^{1}H NMR spectra were recorded using a JNM-ECA-400 spectrometer or a

Bruker Avance 500 MHz spectrometer. 2D NOESY was recorded using a Bruker Avance 600 MHz spectrometer. The single crystal X-ray data were determined by direct methods using SHELXS-97 and refined by full-matrix least-squares procedures on F2 with SHELXL-97. All non-hydrogen atoms were obtained from the difference. Thermogravimetric Analysis (TGA) was recorded using a TA Instrument TA-Q500 and the samples were heated under nitrogen gas at a rate of 10 °C /min. Powder X-ray diffraction (PXRD) data were measured with a powder X-ray diffractometer (D/max 2200vpc, Rigaku, Japan) using Cu Kα radiation (λ = 1.5046 Å) with a range 5–40 °C.

Determination of the association constants. For all the host−guest pairs, chemical exchange is fast on the NMR time scale. To determine the association constant, NMR titrations were done with solutions which had a constant concentration of EtP5 host and varying concentrations of guest. Using the nonlinear curve-fitting method, the association constant was obtained for each host-guest combination from the following equation (Connors, 1987; Shu et al., 2012):

$A = (A_\infty/[H]_0) (0.5[G]_0 + 0.5([H]_0 +1/K_a)-(0.5 ([G]_0^2 + (2[G]_0 (1/K_a − [H]_0)) + (1/K_a + [H]_0)^2)^{0.5})$

where A is the chemical shift change of aromatic proton (H_1 or H_3) on EtP5 host at $[G]_0$, A_∞ is the chemical shift change of H_1 or H_3 when the host is completely complexed, $[H]_0$ is the fixed initial concentration of the host, and $[G]_0$ is the initial concentration of guest. Assuming 1:1 binding stoichiometry between pillar[5]arene host and these guests, the association constants (K_a) could be calculated by using the nonlinear curve-fitting method. For each host−guest pair examined, the plot of Δδ as a function of $[G]_0$ gave an excellent fit, verifying the validity of the 1:1 binding stoichiometry assumed.

Computational method. The binding energies between SM and S1 with EtP5 were calculated by molecular mechanics (MM) calculations. For this purpose, the

geometries of EtP5, SM, S1 and their complexes were separately optimized by ORCA program at the BLYP-D3BJ/def2-TZVP(-f) level (Grimme et al., 2011; Marenich et al., 2009; Weigend et al., 2006). Single point energies of the optimized structures were calculated at the same level.

The binding energy was calculated according to:

$$E_{(bind)} = E_{(complex)} - \{E_{(guest)} + E_{(host)}\}$$

Preparation of EtP5α. Adaptive EtP5α crystal material was obtained by slow evaporation from tetrahydrofuran solution of EtP5, and then desolvated solvent molecules under reduced pressure at 70 °C for 24 h.

Vapor adsorption experiments. For the adsorption experiments, an open 5 mL vial containing 10 mg of EtP5α was placed in a sealed 20 mL vial containing 1 mL SM simulant. EtP5α was exposed under saturated vapor pressure in the closed vessel at 25 °C. Uptake of SM simulants by EtP5α was monitored over time by ^{1}H NMR spectra by completely dissolving the crystals in $CDCl_3$ or CD_2Cl_2.

Supplemental References

Liu, Y., Buru, C. T., Howarth, A. J., Mahle, J. J., Buchanan, J. H., DeCoste, J. B., Hupp, J. T., and Farha, O. K. (2016). Efficient and selective oxidation of sulfur mustard using singlet oxygen generated by a pyrene-based metal–organic framework. J. Mater. Chem. A. 4, 13809–13813.

Xu, B., Zong, C., Nie, Z., Guo, L., and Xie, J. (2014). A novel approach for high sensitive determination of sulfur mustard by derivatization and isotope-dilution LC–MS/MS analysis. Talanta 132, 245–251.

Roy, A., Srivastava, A. K., Singh, B., Mahato, T. H. Shah, D., and Halve, A. K. Degradation of sulfur mustard and 2-chloroethyl ethyl sulfide on Cu–BTC metal organic framework. Microporous and Mesoporous Materials 162, 207–212.

Goud, D. R., Purohit, A. K., Tak, V., Dubey, D. K., Kumar, P., and Pardasani, D. (2014). A highly selective and sensitive "turn-on" fluorescence chemodosimeter for the detection of mustard gas. Chem. Commun. 50, 12363–12366.

Ogoshi, T., Kanai, S., Fujinami, S., Yamagishi, T.-a., and Nakamoto, Y. (2008). *para*-Bridged symmetrical pillar[5]arenes: their lewis acid catalyzed synthesis and host–guest property. J. Am. Chem. Soc. 130, 5022–5023.

Hu, X.-B., Chen, Z., Chen, L., Zhang, L., Hou, J.-L., and Li, Z.-T. (2012). Pillar[*n*]arenes (*n* = 8–10) with two cavities: synthesis, structures and complexing properties. Chem. Commun. 48, 10999–11001.

Connors, K. A. Binding Constants, Wiley: New York (1987).

Grimme, S., Ehrlich, S., and Goerigk, L. (2011). Effect of the damping function in dispersion corrected density functional theory. J Comput Chem, 32, 1456–1465.

Marenich, A. V., Cramer, C. J., and Truhlar, D. G. (2009). Universal solvation model based on solute electron density and on a continuum model of the solvent defined by the bulk dielectric constant and atomic surface tensions. J. Phys. Chem. B, 113, 6378–6396.

Weigend, F. (2006). Accurate Coulomb-fitting basis sets for H to Rn. Phys. Chem. Chem. Phys. 8, 1057–1065.

Shu, X., Chen, S., Li, J., Chen, Z., Weng, L., Jia, X., and Li, C. (2012). Highly effective binding of neutral dinitriles by simple pillar[5]arenes. Chem. Commun. 48, 2967–2969.